UNIVERSITYOF BIRMINGHAM

University of Birmingham
Research at Birmingham

Kruppel-like factor 5 is essential for the maintenance of barrier function in mouse colon

Liu, Yang; Chidgey, Martyn; Yang, Vincent; Bialkowska, Agnieszka

Document Version
Peer reviewed version

[Link to publication on Research at Birmingham portal](#)

RESEARCH ARTICLE | *Epithelial Biology and Secretion*

Krüppel-like factor 5 is essential for maintenance of barrier function in mouse colon

Yang Liu,[1] Martyn Chidgey,[2] Vincent W. Yang,[1,3] and Agnieszka B. Bialkowska[1]

[1]*Department of Medicine, Stony Brook University School of Medicine, Stony Brook, New York;* [2]*School of Cancer Sciences, University of Birmingham, Birmingham, United Kingdom; and* [3]*Department of Physiology and Biophysics, Stony Brook University School of Medicine, Stony Brook, New York*

Liu Y, Chidgey M, Yang VW, Bialkowska AB. Krüppel-like factor 5 is essential for maintenance of barrier function in mouse colon. *Am J Physiol Gastrointest Liver Physiol* 313: G478–G491, 2017. First published September 1, 2017; doi:10.1152/ajpgi.00172. 2017.—Krüppel-like factor 5 (KLF5) is a member of the zinc finger family of transcription factors that regulates homeostasis of the intestinal epithelium. Previous studies suggested an indispensable role of KLF5 in maintaining intestinal barrier function. In the current study, we investigated the mechanisms by which KLF5 regulates colonic barrier function in vivo and in vitro. We used an inducible and a constitutive intestine-specific *Klf5* knockout mouse models (*Villin-CreER^{T2};Klf5$^{fl/fl}$* designated as *Klf5$^{\Delta IND}$* and *Villin-Cre;Klf5$^{fl/fl}$* as *Klf5$^{\Delta IS}$*) and studied an inducible *KLF5* knockdown in Caco-2 BBe cells using a lentiviral Tet-on system (Caco-2 BBe *KLF5ΔIND*). Specific knockout of *Klf5* in colonic tissues, either inducible or constitutive, resulted in increased intestinal permeability. The phenotype was accompanied by a significant reduction in *Dsg2*, which encodes desmoglein-2, a desmosomal cadherin, at both mRNA and protein levels. Transmission electron microscopy showed alterations of desmosomal morphology in both *KLF5* knockdown Caco-2 BBe cells and *Klf5* knockout mouse colonic tissues. Inducible knockdown of *KLF5* in Caco-2BBe cells grown on Transwell plates led to impaired barrier function as evidenced by decreased transepithelial electrical resistance and increased paracellular permeability to fluorescein isothiocyanate-4 kDa dextran. Furthermore, DSG2 was significantly decreased in *KLF5* knockdown cells, and DSG2 overexpression partially rescued the impaired barrier function caused by *KLF5* knockdown. Electron microscopy studies demonstrated altered desmosomal morphology after *KLF5* knockdown. In combination with chromatin immunoprecipitation analysis and promoter study, our data show that KLF5 regulates intestinal barrier function by mediating the transcription of *DSG2*, a gene encoding a major component of desmosome structures.

NEW & NOTEWORTHY The study is original research on the direct function of a Krüppel-like factor on intestinal barrier function, which is commonly exerted by cell junctions, including tight junctions, adherens junctions, and desmosomes. Numerous previous studies were focused on tight junctions and adherens junctions. However, this study provided a new perspective on how the intestinal barrier function is regulated by KLF5 through DSG2, a component of desmosome complexes.

desmosomes; desmoglein-2

Address for reprint requests and other correspondence: A. B. Bialkowska, Dept. of Medicine, Stony Brook Univ. School of Medicine, HSC T-17, Rm. 090, Stony Brook, NY 11794 (e-mail: agnieszka.bialkowska @stonybrookmedicine.edu).

THE INTEGRITY OF THE gastrointestinal epithelium is under stringent homeostatic control and is often impaired in disease conditions such as inflammatory bowel disease (7, 17). Intestinal barrier function, essential for both selective paracellular permeability to electrolytes and water and defensibility against luminal pathogens, is exerted by the polarized monolayer of epithelial cells, with their paracellular space sealed by different types of cell junctions (7). Intestinal cell junctions are composed of tight junctions, adherens junctions, desmosomes, and gap junctions (9, 36). The formation of the former three types of cell junctions requires the assembly of protein complexes consisting of transmembrane proteins and intracellular proteins. Interaction of the intracellular proteins with cell cytoskeletons is essential for the maintenance of cellular structure and epithelial barrier function (12). Many lines of evidence indicate that loss of cell junction integrity results in intestinal inflammation (11, 23, 35, 37), whereas intestinal barrier function is strengthened by upregulation of cell junction proteins (34, 41).

Cell junctions are membranous protein complexes. Tight junctions are distributed at apical foci on the basolateral membrane of adjoining cells and include single transmembrane proteins and intracellular scaffold proteins. Adherens junctions are distributed on the basolateral membrane and composed of transmembrane cadherins and intracellular armadillo proteins. Like adherens junctions, desmosomes also contain cadherins and armadillo proteins, as well as desmoplakin and other intracellular proteins. Desmosomal cadherins consist of two types of transmembrane proteins, desmocollins and desmogleins, which bind in either a heterotypic (6, 21) or homotypic (20) manner. Among the four human desmoglein species and the three human desmocollin species, human intestinal epithelial cells mainly express desmoglein-2 (DSG2) and desmocollin-2 (DSC2) (30). In addition to supporting a mechanical linkage between epithelial cells, recent studies (14, 31) specifically addressed the contribution of DSG2 in maintaining intestinal barrier function. Antibody against the extracellular domain of DSG2 was reported to adversely affect tight junction integrity and impair intestinal epithelial barrier function in Caco-2 cells, a common in vitro model of intestinal epithelium (31).

Krüppel-like factor 5 (KLF5) is a zinc finger transcription factor abundantly expressed in proliferative tissues. As a multifunctional transcription factor, KLF5 has been shown to promote cell proliferation and tumorigenesis in tissues such as urinary bladder, colon, and lung (3, 18, 27) while it functions

as a tumor suppressor in breast and prostate cancers (4, 5). Recently, it was shown that the roles of KLF5 extend beyond oncoprotein or tumor suppressor activities. For example, KLF5 has been shown to be important for cell differentiation of bladder urothelium (1), perinatal morphogenesis of lung (40), postnatal maturation of eyelids (15), embryonic intestinal villus formation (2), maturation and maintenance of intestinal crypt architecture (22), and proliferation and survival of mouse intestinal epithelial stem cells (25). Furthermore, constitutive *Klf5* overexpression in mouse intestinal tissues resulted in less colonic injury under inflammatory stimulus with dextran sodium sulfate (38). Previous studies from our laboratory explored the role of KLF5 in maintaining intestinal epithelial homeostasis using the constitutive intestine-specific *Klf5* deletion mouse model (*Klf5^{ΔIS}*). *Klf5^{ΔIS}* mice were born at a normal Mendelian ratio, but approximately two-thirds of them died shortly after birth while the remainder survive to adulthood primarily due to incomplete deletion of *Klf5*. Besides disrupted intestinal epithelial architecture, the histology of surviving *Klf5^{ΔIS}* mice showed signs of intestinal inflammation, including the presence of neutrophil exudates in the glands of the colon and infiltration of neutrophils in the epithelium and lamina propria of the small and large intestines. Moreover, the permeability across the intestinal epithelium of *Klf5^{ΔIS}* mice as measured by fluorescein isothiocyanate (FITC)-dextran was significantly higher than that in control mice (22). These results suggest a role for KLF5 in maintaining intestinal epithelial barrier function, although the mechanism by which KLF5 exerts this effect has not been determined. Most studies on the regulation of cellular junction complexes have focused on posttranscriptional mechanisms (as reviewed in Ref. 10); the possibility of transcriptional regulation by a Krüppel-like factor has not yet been explored.

In this study, we used *Klf5^{ΔIND}* and *Klf5^{ΔIS}* mouse models to study the role of KLF5 in maintaining intestinal epithelial barrier function. *Klf5* knockout was achieved with five consecutive days of tamoxifen injection to *Klf5^{ΔIND}* mice. The *Klf5*-deleted mice showed reduced intestinal barrier function as characterized by increased permeability to small-molecule FITC-4 kDa dextran. Using quantitative PCR to analyze the expression levels of cell junction components, we found that *Dsg2* gene had the greatest degree of downregulation and similar expression pattern to that of *Klf5*. The absence of DSG2 in *Klf5*-depleted colonic tissues resulted in disrupted desmosomal morphology. Similar phenotype was observed with the *Klf5^{ΔIS}* mouse model. Consistently, *KLF5* knockdown Caco-2 BBe cells showed impaired barrier function, as characterized by reduced transepithelial electrical resistance (TEER) and increased permeability to FITC-4 kDa dextran. DSG2 level was reduced and its distribution was disrupted in *KLF5* knockdown Caco-2 BBe cells as well. The absence of DSG2 in *KLF5* knockdown cells resulted in disrupted desmosomal morphology. Similar phenotype was observed with *DSG2* knockdown Caco-2 BBe cells, whereas *DSG2* overexpression in *KLF5* knockdown cells partially rescued epithelial barrier function. Chromatin immunoprecipitation (ChIP) on the promoter sequences covering the potential binding sites further verified the interaction of KLF5 and *DSG2* promoter. In addition, sequence analysis of *DSG2* promoter identified three potential binding sites of KLF5, and mutations of the potential binding sites impaired KLF5-mediated activation of *DSG2* promoter. Our study is the first to demonstrate that KLF5 maintains intestinal barrier function by controlling expression of a gene encoding an essential desmosomal protein.

MATERIALS AND METHODS

Mice. All animal studies were performed following the protocols approved by Stony Brook University Institutional Animal Care and Use Committee. C57BL/6 mice carrying *Klf5* alleles flanked by loxP sites were crossed with *Villin-CreER^{T2}* or *Villin-Cre* mice carrying the Cre recombinase gene fused with or without estrogen receptor T2 gene under regulation of *Villin* promoter to generate *Villin-CreER^{T2}; Klf5^{fl/fl}* (*Klf5^{ΔIND}*) or *Villin-Cre;Klf5^{fl/fl}* (*Klf5^{ΔIS}*) mice, respectively, as previously described (22). Eight-week-old *Villin-CreER^{T2}* and *Klf5^{ΔIND}* mice were injected with corn oil or 1 mg of tamoxifen dissolved in 100 μl of corn oil for five consecutive days before being sacrificed on the 6th day since the first dose. Five-week-old *Villin-Cre* and *Klf5^{ΔIS}* mice were sacrificed and tissue was collected on *day 37* after birth.

Cell culture reagents. Caco-2 BBe and HEK 293T cells were purchased from the ATCC (Manassas, VA). Caco-2 BBe and HEK 293T cells were maintained in Dulbecco's modified Eagle's medium (Cellgro, Manassas, VA) supplemented with 10% fetal bovine serum (Atlanta Biologicals, Norcross, GA) and 1% penicillin-streptomycin (ThermoFisher Scientific, Waltham, MA).

Establishment of inducible KLF5 knockdown or inducible DSG2 knockdown in Caco-2 BBe cells. The inducible short-hairpin RNA (shRNA) expression plasmid pLKO.1-tet-on was obtained from Addgene (Cambridge, MA) (42). The plasmids encoding shRNAs (pLKO.1-tet-on-KLF5shRNA and pLKO.1-tet-on-DSG2shRNA) were generated by ligation of the following oligonucleotides: shKLF5 sense 5′-CCGGCCCTGCCAGTTAACTCACAAACTCGAGTTT-GTGAGTTAACTGGCAGGGTTTTT-3′ and shKLF5 antisense 5′-AATTAAAAACCCTGCCAGTTAACTCACAAACTCGAGTTT-GTGAGTTAACTGGCAGGG-3′ or shDSG2 sense 5′-CCGGCCTT-ATTAAGGAAGTAGATTACTCGAGTAATCTACTTCCTTAA-TAAGGTTTTT-3′ and shDSG2 antisense 5′-AATTAAAAACCT-TATTAAGGAAGTAGATTACTCGAGTAATCTACTTCCTTA-ATAAGG-3′ into pLKO.1-tet-on plasmid digested with *Age*I and *Eco*RI enzymes. pCD/NL-BH* ΔΔΔ and pLTR-G plasmids were kindly provided by Dr. Jakob Reiser (Food and Drug Administration, Silver Spring, MD). Vector particles were produced in HEK 293T cells by transient cotransfection with modifications as previously described (16). Briefly, HEK 293T cells were plated on 100-mm plates in 15 ml of medium (2 × 10^6 cells/plate) and 24 h later transfected with pLKO.1-tet-on-KLF5shRNA, pLKO.1-tet-on-DSG2shRNA, or pLKO.1-tet-on plasmid DNA (7.5 μg), pCD/NL-BH* ΔΔΔ helper plasmid DNA (5 μg), and pLTR-G DNA (2.5 μg) using Lipofectamine 2000 (ThermoFisher Scientific). The medium was replaced, and virus particles released in the medium were harvested 16 h after transfection. Caco-2 BBe cells (2 × 10^5 cells/well) were plated on six-well plates, and 24 h later pLKO.1-tet-on-KLF5shRNA, pLKO.1-tet-on-DSG2shRNA, or pLKO.1-tet-on viruses were added in medium containing 8 μg/ml of polybrene (Sigma, St. Louis, MO). Antibiotic-resistant colonies were selected in medium containing 4 μg/ml of puromycin dihydrochloride (Santa Cruz Biotechnology, Dallas, TX) for two weeks. Clones of puromycin-resistant colonies were pooled as the stable transduced control Caco-2 BBe cell line (Caco-2 BBe pLKO.1), the stable inducible *KLF5* knockdown Caco-2 BBe cell line (Caco-2 BBe *KLF5ΔIND*), or the stable inducible *DSG2* knockdown Caco-2 BBe cell line (Caco-2 BBe *DSG2ΔIND*).

Establishment of DSG2 overexpression in Caco-2 BBe KLF5 ΔIND cells. The DSG2 lentiviral activation particles and control lentiviral activation particles were purchased from Santa Cruz Biotechnology. Caco-2 BBe *KLF5ΔIND* cells (2 × 10^5 cells/well) were seeded in six-well plates and 24 h later transfected with DSG2 or control

Table 1. *List of antibodies used for Western blot analysis and immunofluorescence staining*

Antibodies	Catalog No. and Company	Western Blot Analysis	IF Staining
Rabbit anti-KLF5	sc-22797, Santa Cruz Biotechnology	1:1,000 diluted in 5% milk	1:200 diluted in 10% horse serum
Goat anti-KLF5	AF3758, R&D	N/A	1:100 diluted in 1% milk
Rabbit anti-DSG2	GTX102508, GeneTex	1:1,000 diluted in 5% milk	1:200 diluted in 10% horse serum
Rabbit anti-DSG2	AB150372, Abcam	N/A	1:200 diluted in 1% milk
Sheep anti-DSC2	AF4688, R&D	1:1,000 diluted in 5% milk	1:100 diluted in 10% horse serum for immunocytochemistry 1:100 diluted in 1% milk for immunohistochemistry
Mouse anti-GAPDH	MAB374, EMD Millipore	1:5,000 diluted in 5% milk	N/A

IF, immunofluorescence; KLF5, Krüppel-like factor 5; DSG, desmoglein-2; DSC2, desmocollin-2; N/A, not applicable.

lentiviral activation particles in medium containing 8 μg/ml of polybrene (Sigma). Antibiotic-resistant colonies were selected in medium containing 4 μg/ml of puromycin dihydrochloride, 300 μg/ml of Hygromycin B, and 1 μg/ml Blasticidin S hydrochloride (Santa Cruz Biotechnology) for two weeks. Clones of antibiotic-resistant colonies were picked and expanded as the stable *DSG2* overexpression Caco-2 BBe *KLF5ΔIND* cell line (Caco-2 BBe *KLF5ΔIND DSG2*) or the control cell line (Caco-2 BBe *KLF5ΔIND EV*).

Transepithelial electrical resistance measurement and paracellular permeability assay. Caco-2 BBe cell lines were maintained in DMEM containing 10% FBS and 1% penicillin-streptomycin with 4 μg/ml puromycin dihydrochloride. Caco-2 BBe cells were seeded in the permeable Transwell inserts (0.4 μm pore size, 12 mm diameter; Corning, Pittston, PA) at the density of 7×10^4 cells/well. To induce the expression of shRNAs, doxycycline hydrochloride (Sigma Aldrich) was added to the medium on *day 3* of the culture and maintained for the remaining days of cell culture. The transepithelial electrical resistance of the Caco-2 BBe monolayers was measured every 3 or 4 days with an EVOM epithelial voltohmmeter and ENDOHM-12 chamber (World Precision Instruments, Sarasota, FL) using PBS as electrolyte. TEER is expressed by multiplying the resistance with growth area of the inserts ($\Omega \cdot cm^2$). To measure paracellular permeability, at the end point of the 28-day cell culture, 500 μl of Hanks' Balanced Salt Solution (HBSS; Cellgro) containing 1 mg/ml FITC-4 kDa dextran (Sigma) were added to the apical chambers, and 1.5 ml of HBSS in the basal chambers of the Transwell plate, and then incubated in the CO_2 incubator for 4 h. Mice were gavaged with 1 mg of FITC-4 kDa dextran solution 4 h before euthanization. Cardiac blood was drawn, left coagulating for 30 min at room temperature, and centrifuged to separate serum from blood cells. The pass-through concentration of the fluorescent molecule in HBSS or serum was quantified using a SpectraMax M3 microplate reader (Molecular Devices, Sunnyvale, CA) with the following settings: wavelength of excitation = 485 nm, wavelength of emission = 525 nm.

Western blot analysis. Cells were lysed in 1× Laemmli Buffer, and proteins were resolved by SDS-PAGE and blotted on nitrocellulose membrane. Blots were blocked with 5% nonfat milk dissolved in 50 mM Tris, 150 mM NaCl, and 0.05% Tween 20, pH 7.6 (TBST), buffer for 1 h at room temperature. The membranes were incubated at 4°C overnight with antibodies as listed in Table 1. Following washes with TBST, membranes were then incubated with appropriate unconjugated secondary antibodies at room temperature for 1 h and then incubated with appropriate horseradish peroxidase (HRP)-conjugated tertiary antibodies after washes in between. For the probing of GAPDH, only HRP-conjugated secondary antibody was used. The membranes were washed with TBST and incubated with HRP substrate for 2 min followed by film development.

Immunofluorescence staining. Paraffin-embedded *Villin-CreER^{T2}*, *Klf5ΔIND*, *Villin-Cre*, and *Klf5ΔIS* tissue sections were rehydrated with xylene and ethanol gradients and pressure cooked to expose the antigen epitope. Sections were blocked with 1% nonfat milk in Tris-Tween-buffered saline and incubated with antibodies listed in Table 1. Unconjugated chicken anti-rabbit and Alexa 488-labeled

donkey anti-chicken were diluted at 1:300 to detect KLF5 and DSG2 but unconjugated bovine anti-goat and Alexa-594 labeled goat anti-bovine diluted at 1:300 to probe KLF5 and DSC2. The DNA was counterstained with Hoechst dye. The fluorescence was visualized using a Nikon Eclipse 90i microscope (Nikon), and images were acquired and processed with NIS-Elements.

Caco-2 BBe cell lines that had been grown in Transwell inserts for 28 days were fixed with 3.7% paraformaldehyde and washed with PBS. Epithelial monolayers were blocked with 10% horse serum (ThermoFisher Scientific) in PBS at 37°C for 1 h and incubated at 4°C overnight with primary antibodies listed in Table 1. Alexa 488-conjugated goat anti-rabbit antibody diluted 1:300 was used to visualize proteins at 37°C for 1 h. DNA was counterstained with 1 μM TO-PRO3 iodide (ThermoFisher Scientific) for 10 min at room temperature, and then samples were mounted using the Prolong Gold anti-fade mounting medium (ThermoFisher Scientific) and stored at −20°C in the dark until analyzed. The fluorescence was visualized using a Zeiss 510 confocal microscope, and images were acquired and processed with the LSM 5 Image Browser.

Quantitative RT-PCR. Total RNA was extracted from fresh mouse tissues using the RNeasy Mini kit (Qiagen, Valencia, CA) in combination with the RNase-free DNase Set (Qiagen) according to the manufacturer's instructions. cDNA was synthesized using the Superscript VILO cDNA synthesis kit (ThermoFisher Scientific). Quantitative PCR with mouse colonic tissues was performed in triplicates with primer sets for *Hprt1* (catalog no. QT00166768; Qiagen), *Klf5* (catalog no. QT01057756; Qiagen), *Dsg2* (catalog no. QT00173257; Qiagen), *Dsc2* (catalog no. QT00156198; Qiagen), *Cdh1*, *Ctnna1*, *Ctnnb1*, *Tjp1*, *Ocln*, *F11r*, *Cldn2*, and *Cldn4* (primer sequences are listed in Table 2). Products were amplified and detected with the Power SYBR PCR Master Mix (ThermoFisher Scientific) on an Eppendorf REALPLEX ep gradient S real-time PCR Mastercycler according to the manufacturer's instructions. Relative changes in

Table 2. *List of primer sequences used for quantitative RT-PCR*

Target Gene	Primer Sequence
Cadherin 1 (Cdh1)	Forward: 5′-CAGGTCTCCTCATGGCTTTGC-3′
	Reverse: 5′-CTTCCGAAAAGAAGGCTGTCC-3′
Catenin-α₁ (Ctnna1)	Forward: 5′-AAGTCTGGAGATTAGGACTCTGG-3′
	Reverse: 5′-ACGGCCTCTCTTTTTTATTAGACG-3′
Catenin-β₁ (Ctnnb1)	Forward: 5′-ATGGAGCCGGACAGAAAAGC-3′
	Reverse: 5′-CTTGCCACTCAGGGAAGGA-3′
Tight junction protein 1 (Tjp1)	Forward: 5′-ACCACCAACCCGAGAAGAC-3′
	Reverse: 5′-CAGGAGTCATGGACGCACA-3′
Occludin (Ocln)	Forward: 5′-TTGAAAGTCCACCTCCTTACAGA-3′
	Reverse: 5′-CCGGATAAAAAGAGTACGCTGG-3′
F11 receptor (F11r)	Forward: 5′-TCTCTTCACGTCTATGATCCTGG-3′
	Reverse: 5′-TTTGATGGACTCGTTCTCGGG-3′
Claudin 2 (Cldn2)	Forward: 5′-CAACTGGTGGGCTACATCCTA-3′
	Reverse: 5′-CCCTTGGAAAAGCCAACCG-3′
Claudin 4 (Cldn4)	Forward: 5′-GTCCTGGGAATCTCCTTGGC-3′
	Reverse: 5′-TCTGTGCCGTGACGATGTTG-3′

expression were calculated based on the comparative C_T ($-\Delta\Delta C_T$) method (32) after normalization to *Hprt1* control.

Transmission electron microscopy. Colonic tissues isolated from *Villin-CreER^T2*, *Klf5^ΔIND*, *Villin-Cre*, and *Klf5^ΔIS* mice and Caco-2 BBe cell lines that had been grown in Transwell inserts for 28 days were fixed at 4°C overnight in 2.5% electron microscopy-grade glutaraldehyde (Electron Microscopy Sciences, Hatfield, PA) in 0.1 M PBS, pH 7.4. Samples were processed, and sections were prepared by the Central Microscopy Imaging Center at Stony Brook University. Sections were viewed with an FEI Tecnai12 BioTwinG² transmission electron microscope. Images were acquired with an AMT XR-60 CCD digital camera system and assembled using ImageJ software (33).

Chromatin immunoprecipitation. Human *DSG2* 5′-flanking DNA was amplified by PCR from yeast artificial chromosome clone 9G-C3 (Source BioScience). Plasmid pGL3BDSG2(500) contained bases -500 to -1 of *DSG2* 5′-flanking DNA. Because of low transfection efficiency of the Caco-2 BBe cell line, 1×10^7 HEK 293T cells instead were seeded in a 150-mm culture dish and transfected with plasmids pMT3-HA-KLF5 and pGL3BDSG2(500). Later (24 h), cells were cross-linked with 37% formaldehyde and lysed, DNA was sheared (200–1,000 bp) by sonication, and fragments were incubated with human influenza hemagglutinin (HA) antibody (Cell Signaling Technology) and KLF5 rabbit polyclonal antibody developed by our laboratory. The specific KLF5-binding regions were enriched with the ChIP assay kit (Millipore, Billerica, MA) according to the manufacturer's protocol. Amplification of *DSG2* promotor sequence bound to KLF5 was accomplished by PCR using the following primers: site 1 forward: 5′-TACTTGGTCCCGCAGGACTCT-3′, reverse: 5′-CCCAAGGACAAAAGCTCCA-3′; site 2 + 3 forward: 5′-GCTTTTGTCCTTGGGCCG-3′, reverse: 5′-ACTCTCTGGAG-AATGGCGG-3′. DNA electrophoresis was performed in 4% agarose gels.

DSG2 promoter analysis. Human *DSG2* 5′-flanking DNA was subcloned into the pLightSwitch promoter reporter vector (ActiveMotif, Carlsbad, CA) digested with *KpnI* and *XhoI*. Site-directed mutagenesis was used to generate KLF5-binding site mutations MUT1, MUT2, and MUT3. Because of low transfection efficiency of the Caco-2 BBe cell line, HEK 293T cells instead were seeded in 96-well plates at the density of 1×10^4 cells/well. Cells were transfected at 70% confluence with pLightSwitch, pLightSwitch-DSG2(500), or KLF5-binding site mutant constructs, in combination with pEGFP-ΔEGFP or pEGFP-ΔEGFP-KLF5-HA, using Lipofectamine 2000. Later (1 day), luciferase activities were determined with the LightSwitch Luciferase Assay System (Active Motif). The firefly luciferase activity was quantified using a luminometer.

Statistical analysis. Statistical analysis was performed using GraphPad Prism version 4.0 for Windows (GraphPad Software).

RESULTS

Dsg2 level and Dsc2 level are reduced in the colon of mice with intestine-specific deletion of Klf5. To investigate the relationship between KLF5 and intestinal barrier function in vivo we used the *Klf5^ΔIND* mouse model. We injected *Klf5^ΔIND* mice with 1 mg tamoxifen for five consecutive days to induce *Klf5* knockout (Fig. 1*A*) and collected and analyzed the tissues. This time point represents the most severe phenotype in *Klf5^ΔIND* mice as previously reported (26). Female *Klf5^ΔIND* mice were more susceptible to *Klf5* knockout than male *Klf5^ΔIND* mice because of higher efficiency of *Klf5* depletion (unpublished data) and demonstrated significant pathogenesis, characterized by anal bleeding and decreased body weight compared with their littermates injected with corn oil for five consecutive days and with *Villin-CreER^T2* mice injected with corn oil or 1 mg tamoxifen for five consecutive days. We observed gender-dependent efficiency of *Klf5* deletion upon tamoxifen treatment, with female mice demonstrating greater level of KLF5 reduction by qPCR and immunohistochemistry (data not shown). FITC-dextran permeability assay was performed by gavage 4 h before collecting cardiac blood and measuring FITC signal in serum. A threefold increase in FITC concentration in serum was observed in female mice with deleted *Klf5* in intestines, whereas no changes in FITC-dextran concentration in serum were observed between *Villin-CreER^T2* control mice treated with or without tamoxifen induction (Fig. 1*B*). We collected RNA from colonic tissues of corn oil-injected and tamoxifen-injected mice and analyzed the levels of cell junction component genes, such as *Cdh1*, *Ctnna1*, *Ctnnb1*, *Tjp1*, *Ocln*, *F11r*, *Cldn2*, *Cldn4*, *Dsg2*, and *Dsc2*. As shown in Fig. 1*C*, both *Dsg2* and *Dsc2* mRNA levels in tamoxifen-treated *Klf5^ΔIND* mice were significantly reduced compared with corn oil-treated mice but not altered in the *Villin-CreER^T2* controls, whereas other cell junction genes did not have the same response to *Klf5* knockout as *Dsg2* and *Dsc2*. Reduced levels of *Dsg2* mRNA and *Dsc2* mRNA were accompanied by decreased levels of DSG2 and DSC2 proteins, respectively, as indicated by immunofluorescence double staining of KLF5 and DSG2 or DSC2 (Fig. 1*D*). DSG2 and DSC2 are the major desmosomal cadherin species expressed in intestinal epithelium (30). DSG2 is a cell junction protein that is highly expressed in the intestinal epithelium, and several lines

Fig. 1. Desmoglein-2 (DSG2) and desmocollin-2 (DSC2) are reduced and mislocalized, and accompanied by altered morphology of desmosomes in the colonic tissue of tamoxifen-induced female *Villin-CreER^T2;Klf5^fl/fl* (*Klf5^ΔIND*) mice compared with the corn oil-injected control group, and *Villin-CreER^T2* mice. *A*: qPCR analysis of Krüppel-like factor 5 (*Klf5*) mRNA expression levels was determined in corn oil-injected or tamoxifen-injected female *Villin-CreER^T2* and *Klf5^ΔIND* mice, respectively. Data represent means ± SE ($n = 8$), *$P < 0.05$ and ***$P < 0.001$ by Student's *t*-test. *B*: fluorescein isothiocyanate (FITC)-dextran concentrations in serum 4 h after gavage of 1mg FITC-4 kDa dextran solution. Data represent means ± SE ($n = 8$), *$P < 0.05$ by Student's *t*-test. *C*: qPCR analysis of *Cdh1*, *Ctnna1*, *Ctnnb1*, *Tjp1*, *Ocln*, *F11r*, *Cldn2*, *Cldn4*, *Dsg2*, and *Dsc2* mRNA expression levels was performed on tissues from corn oil-injected and tamoxifen-injected female *Villin-CreER^T2* or *Klf5^ΔIND* mice. Data represent means ± SE ($n = 8$), **$P < 0.01$ by Student's *t*-test. *D*: immunofluorescence staining of KLF5 (red) and DSG2 (green) (*a*–*h*), and KLF5 (green) and DSC2 (red) (*i*–*p*) in proximal colon and distal colon of corn oil-injected and tamoxifen-injected *Villin-CreER^T2* and *Klf5^ΔIND* mice, respectively. DNA was counterstained with Hoechst dye. Images were taken at ×200 magnification. Scale bars in proximal sections indicate 20 μm, whereas scale bars in distal sections indicate 50 μm. Yellow arrowheads indicate DSG2 or DSC2 staining on basolateral membranes on the epithelial surface, whereas white arrowheads indicate DSG2 or DSC2 staining on the apical sides of the basolateral membranes in crypts. Relative mean fluorescence intensity was quantified (*q* and *r*). Data represent means ± SE ($n = 10$), *$P < 0.05$, **$P < 0.01$, and ***$P < 0.001$ by Student's *t*-test. *E*: transmission electron microscopy images showing changes in morphology of desmosomes in *Klf5*-depleted colonic tissue (*d*, ×30,000 magnification) compared with the controls (*a*–*c*, ×30,000 magnification). White arrows indicate apical junctional complexes; yellow arrowheads indicate desmosomes. Scale bars indicate 400 nm. *F*: quantitative analysis of the number of desmosomes in colonic cells of corn oil- or tamoxifen-injected *Villin-CreER^T2* and *Klf5^ΔIND* mice. Data represent means ± SE ($n = 6$ for corn oil-injected *Villin-CreER^T2*, $n = 5$ for tamoxifen-injected *Villin-CreER^T2*, and $n = 8$ for *Klf5^ΔIND*), ***$P < 0.001$, Student's *t*-test. *G*: quantitative analysis of the width of the intercellular spaces between desmosomes in colonic cells of corn oil- or tamoxifen-injected *Villin-CreER^T2* and *Klf5^ΔIND* mice. Data represent means ± SE ($n = 37$ for corn oil-injected *Villin-CreER^T2*, $n = 29$ for tamoxifen-injected *Villin-CreER^T2*, $n = 42$ for corn oil-injected *Klf5^ΔIND*, and $n = 15$ for tamoxifen-injected *Klf5^ΔIND*), **$P < 0.01$, Student's *t*-test.

of evidence have demonstrated a positive correlation between DSG2 and barrier function (31, 35). In control mice, DSG2 staining was observed on both apical and basolateral compartments of the membrane of epithelial cells on the epithelial surface in colon, whereas DSG2 staining at the apical membrane of epithelial cells was observed only in colonic crypts (Fig. 1D, a–f). The immunofluorescence staining of DSG2 showed that its staining intensity is significantly reduced on the apical membrane of epithelial cells in colonic crypts of tamoxifen-treated $Klf5^{\Delta IND}$ mice with diminished KLF5 staining (Fig. 1D, g and h) compared with control mice, which was

verified by quantification of fluorescence intensity (Fig. 1Dq). Immunofluorescence staining of DSC2 in corn oil (Fig. 1D, m and n)- and tamoxifen-injected $Klf5^{\Delta IND}$ mouse colonic tissues showed a significant reduction of DSC2 level and redistribution in proximal colon sections (Fig. 1Do) and only redistribution in distal colon sections (Fig. 1Dp), also verified by quantification of fluorescence intensity (Fig. 1Dr). These results demonstrate that KLF5 is required for the maintenance of intestinal barrier function and that the level and pattern of both $Dsg2$ and $Dsc2$ expression depend on the presence of KLF5 in the $Klf5^{\Delta IND}$ mouse model. We examined the morphology of
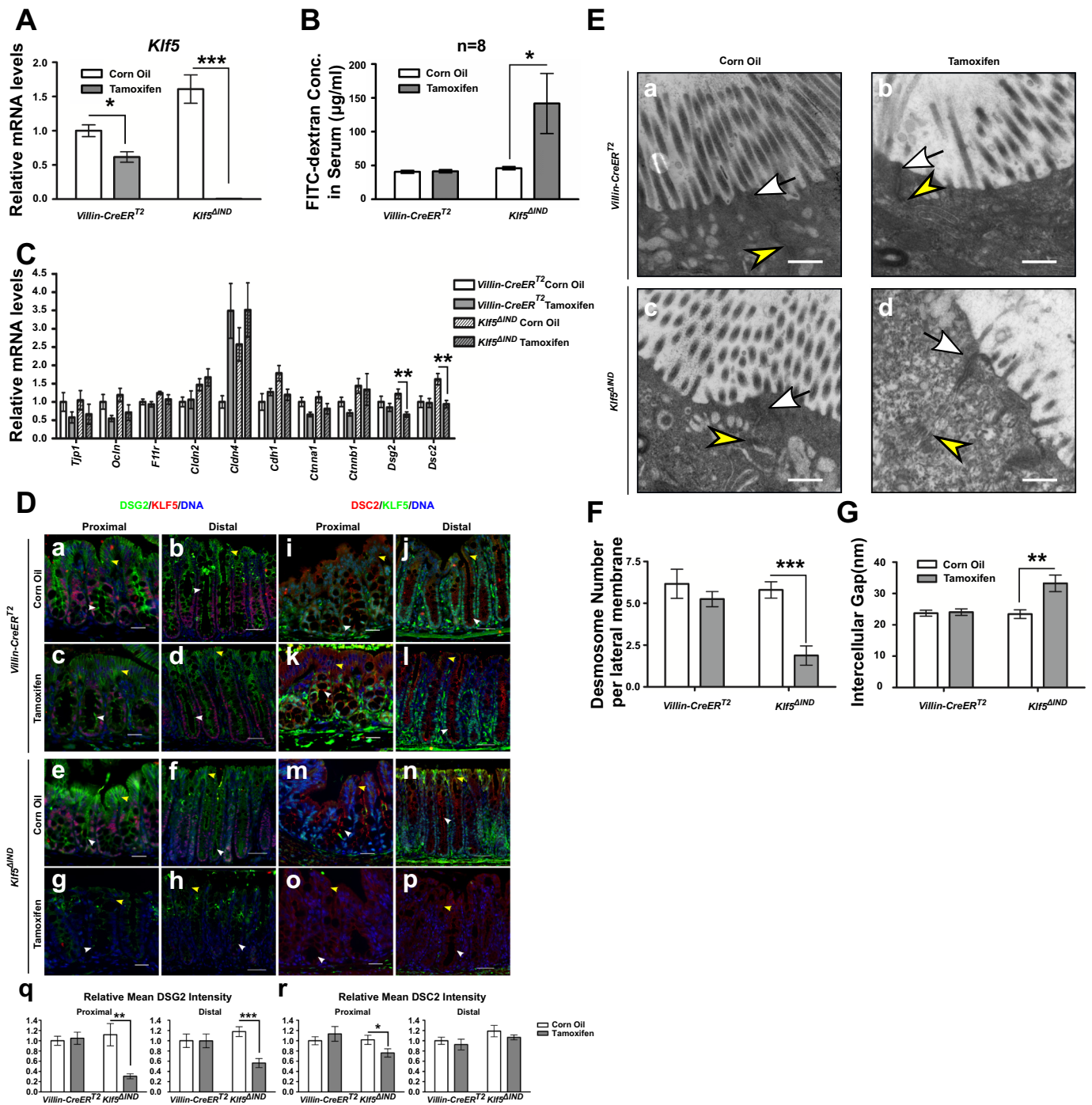
desmosomes in the colonic tissues of the animals using transmission electron microscopy (TEM). The colonic cells of *Villin-CreER^{T2}* mice and corn oil-injected *Klf5^{ΔIND}* mice fully polarized in epithelial cells with abundant brush borders on the apical surface, apical junctional complexes, and numerous desmosomes (apical foci demonstrated in Fig. 1*E*). In contrast, the colonic cells in tamoxifen-injected *Klf5^{ΔIND}* mice showed dramatic alteration in desmosomal morphology: the number of brush-border microvilli on the apical membranes was decreased (Fig. 1*Ed*). Furthermore, the structures of desmosomes were disrupted in *Klf5*-depleted cells, manifested by decreased desmosome numbers and an enlarged intercellular space between adjacent plasma membranes. We further quantified the number of desmosomes on the basolateral membrane. The average number of desmosomes on each basolateral plasma membrane per section was close to six in *Villin-CreER^{T2}* controls and corn oil-injected *Klf5^{ΔIND}* mice, but the number was reduced to two in tamoxifen-injected *Klf5^{ΔIND}* mice (Fig. 1*F*). The average width of intercellular gap between desmosome plaques of cells in tamoxifen-injected *Klf5^{ΔIND}* mice was ~40% wider than those of the controls (Fig. 1*G*). In contrast, the structure and distribution of apical junctional complexes were maintained upon *Klf5* knockout. These results suggest that the observed changes in epithelial morphology resulting from KLF5 loss could be attributed to decreased numbers of desmosomes and structural alterations.

Previous studies demonstrated increased gut permeability using FITC-dextran assay in the *Klf5^{ΔIS}* mouse model regardless of gender (22). Two-thirds of *Klf5^{ΔIS}* mice died shortly after birth, whereas adult surviving mice were sacrificed on *day 37* after birth when they demonstrated severe characteristics of *Klf5* knockout as previously reported. We analyzed mRNA levels of *Klf5*, *Dsg2*, and *Dsc2* and discovered that *Dsg2* mRNA level was significantly reduced and *Dsc2* mRNA level had an insignificant reduction in *Klf5* knockout mouse tissues compared with control tissues (Fig. 2*A*). Using immunofluorescent staining, we observed that DSG2 staining was altered in *Klf5^{ΔIS}* distal colon (Fig. 2*Bd*) in the same pattern as observed in tamoxifen-injected female *Klf5^{ΔIND}* mouse colons. The quantification of fluorescence intensity demonstrated that DSG2 levels were significantly reduced in *Klf5^{ΔIS}* distal colon sections compared with the control, whereas the reduction was not significant in proximal sections (Fig. 2*Bi*). However, DSC2 staining intensities (Fig. 2*Bj*) and patterns are not obviously different between *Klf5^{ΔIS}* and *Villin-Cre* tissues (Fig. 2*B, e–h*), which is consistent with the lack of significant decrease in its mRNA levels (Fig. 2*A*). Similar morphological changes illustrated by TEM are shown in Fig. 2*C*, and similar changes in desmosome number and intercellular gap between desmosomal plaques are shown in Fig. 2, *D* and *E*, respectively.

KLF5 is required for the maintenance of epithelial barrier function in Caco-2 BBe cells. To confirm the role of KLF5 in maintaining epithelial barrier function in vitro, we established an inducible *KLF5* knockdown cell line, Caco-2 BBe *KLF5ΔIND*, as described in MATERIALS AND METHODS. We seeded Caco-2 BBe cells in permeable Transwell plates and grew them for 3 days until confluence was achieved. On the 3rd day of the culture, we added doxycycline to induce expression of *KLF5* shRNAs to commence *KLF5* knockdown. Samples were collected on *day 28* when the TEER values reached the plateau phase in control cells. Western blot analysis of cell

lysates collected from the epithelial cell monolayers confirmed the successful inhibition of KLF5 expression in doxycycline-treated Caco-2 BBe *KLF5ΔIND* but not the control cell line Caco-2BBe pLKO.1 (Fig. 3, *A* and *B*). The development of TEER was significantly impeded in doxycycline-treated Caco-2 BBe *KLF5ΔIND* cells (designated as +DOX) compared with the water-treated Caco-2 BBe *KLF5ΔIND* cells (designated as –DOX), and pLKO.1 groups. TEER reached a plateau of 7.6 $\Omega \cdot cm^2$ on the 28th day of treatment in Caco-2 BBe *KLF5ΔIND* +DOX cells, 27.8 $\Omega \cdot cm^2$ in the Caco-2 BBe *KLF5ΔIND* –DOX cells, 27.8 $\Omega \cdot cm^2$ in the Caco-2 BBe pLKO.1 –DOX cells, and 32.0 $\Omega \cdot cm^2$ in the Caco-2 BBe pLKO.1 +DOX cells (Fig. 3*C*). Consistent with the difference in TEER values on *day 28* of culture, the pass-through concentrations of FITC-4 kDa dextran molecules across the Caco-2 BBe *KLF5ΔIND* +DOX monolayers were approximately fivefold higher than those across the Caco-2 BBe *KLF5ΔIND* –DOX monolayers, whereas the pLKO.1 group did not show significant differences between +DOX and –DOX treatments (Fig. 3*D*). These results demonstrate that *KLF5* knockdown diminishes the integrity of barrier function of Caco-2 BBe cells, resulting in increased permeability.

DSG2 but not DSC2 expression is significantly reduced in KLF5 knockdown Caco-2 BBe cells. To assess the difference in protein levels of DSG2 and DSC2, we analyzed protein extracts from Caco-2 BBe *KLF5ΔIND* –DOX and Caco-2 BBe *KLF5ΔIND* +DOX cells cultured for 28 days in Transwell plates. Our results show that DSG2 protein levels were significantly lower in Caco-2 BBe *KLF5ΔIND* +DOX compared with control, whereas DSC2 protein levels were not changed (Fig. 4, *A* and *B*). Furthermore, we confirmed the absence of DSG2 and the unaltered expression and distribution of DSC2 in Caco-2 BBe *KLF5ΔIND* +DOX cells using immunofluorescence staining. In contrast to specific localization of DSG2 on basolateral membranes in Caco-2 BBe *KLF5ΔIND* –DOX cells as well as Caco-2 pLKO.1 –DOX and +DOX cells, we observed negligible staining in Caco-2 BBe *KLF5ΔIND* +DOX cells (Fig. 4*C, d* and *i*). However, DSC2 is distributed on basolateral membranes in Caco-2 BBe *KLF5ΔIND* –DOX cells as well as pLKO.1 –DOX and +DOX cells (Fig. 4*C, e–g*) but slightly redistributed to the cytoplasm of Caco-2 BBe *KLF5ΔIND* +DOX cells (Fig. 4*Ch*). The fluorescence intensity quantification did not show a statistically significant difference in DSC2 level between controls and *KLF5* knockdown cells (Fig. 4*Cj*). Taken together these results show that knockdown of *KLF5* decreases *DSG2* expression but does not affect DSC2 protein level.

Desmosome structure is disrupted in Caco-2 BBe KLF5ΔIND +DOX cells. DSG2 and DSC2 are two major transmembrane desmosomal cadherin proteins expressed in human intestinal epithelium (30). Therefore, the loss of DSG2 could affect the structure or number of desmosomes in the intercellular junctions. We examined the morphology of desmosomes in Caco-2 BBe *KLF5ΔIND* –DOX and *KLF5ΔIND* +DOX cells after 28 days of growth in permeable inserts using TEM. The Caco-2 BBe *KLF5ΔIND* –DOX and pLKO.1 –DOX and +DOX cells fully polarized into columnar epithelial cells with abundant brush borders on the apical surface, apical junctional complexes, and numerous desmosomes (apical foci demonstrated in Fig. 4*D, a–c*). In contrast, the epithelial monolayers of Caco-2 BBe *KLF5ΔIND* +DOX cells showed dramatic alteration in morphology (Fig. 4*Dd*). Caco-2 BBe
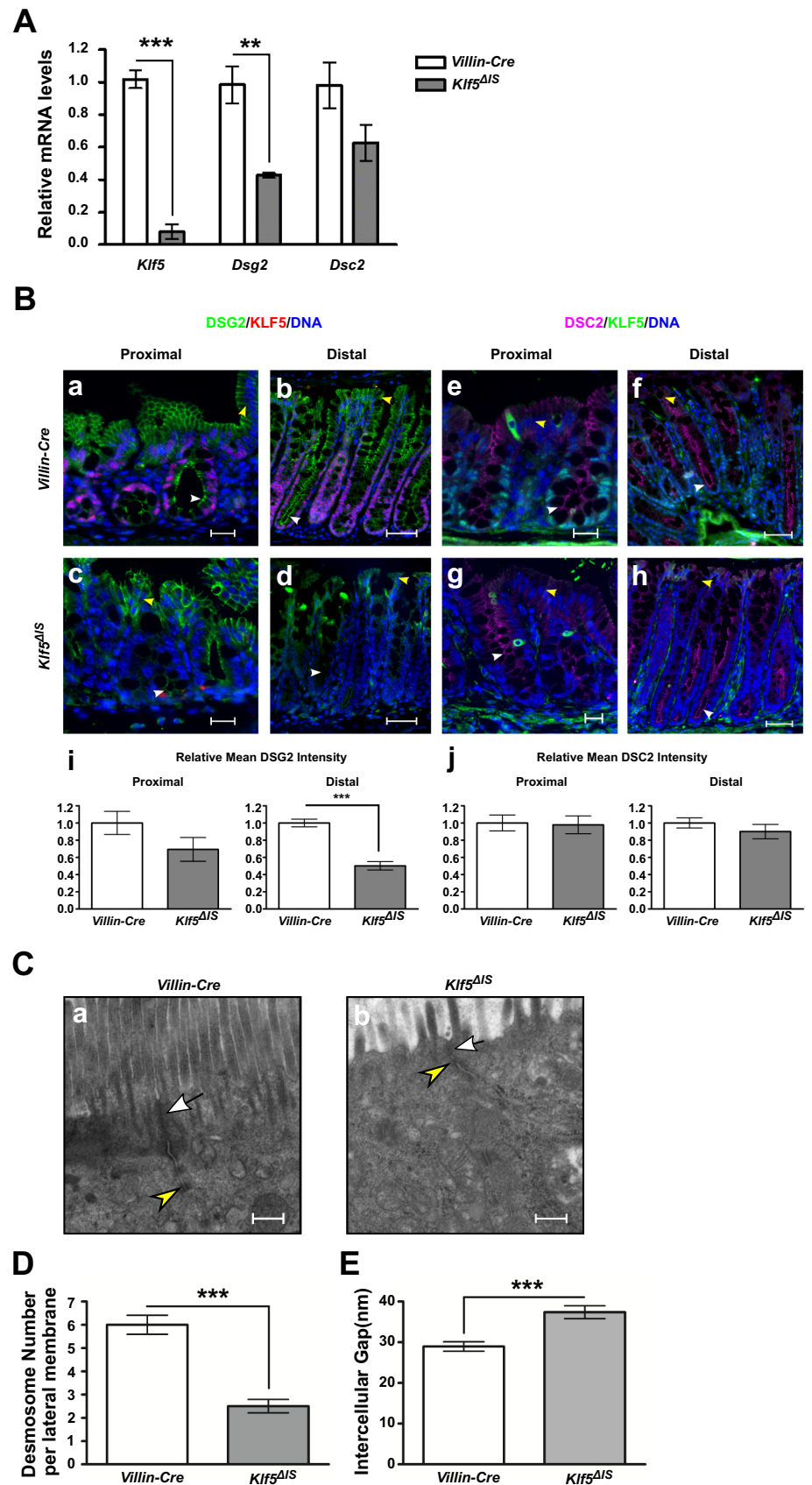
Fig. 2. DSG2 is reduced and mislocalized and morphology of desmosomes is altered in the colonic tissue of $Klf5^{\Delta IS}$ mice. *A*: qPCR analysis of *Klf5, Dsg2*, and *Dsc2* mRNA expression levels was performed on tissues from in *Villin-Cre* mice and $Klf5^{\Delta IS}$ mice. Data represent means ± SE ($n = 6$ for control, and $n = 5$ for $Klf5^{\Delta IS}$), **$P <$ 0.01 and ***$P < 0.001$ by Student's *t*-test. *B*: immunofluorescence staining of KLF5 (magenta) and DSG2 (green) (*a–d*) and KLF5 (green) and DSC2 (magenta) (*e–h*) in proximal colon and distal colon of control and $Klf5^{\Delta IS}$ mice. DNA was counterstained with Hoechst dye. Images were taken at ×200 magnification. Scale bars in proximal sections indicate 20 μm, whereas scale bars in distal sections indicate 50 μm. Yellow arrowheads indicate DSG2 or DSC2 staining on basolateral membranes on the epithelial surface, whereas white arrowheads indicate DSG2 or DSC2 staining on the apical sides of the basolateral membranes in crypts. Relative mean fluorescence intensity was quantified (*i* and *j*). Data represent means ± SE ($n = 10$), ***$P < 0.001$ by Student's *t*-test. *C*: transmission electron microscopy images showing changes in morphology of desmosomes in *Klf5*-depleted colonic tissue (*a*, ×30,000 magnification) compared with the control (*b*, ×30,000 magnification). White arrows indicate apical junctional complexes; yellow arrowheads indicate desmosomes. Scale bars indicate 400 nm. *D*: quantitative analysis of the number of desmosomes in colonic cells of *Villin-Cre* and $Klf5^{\Delta IS}$ mice. Data represent means ± SE ($n = 4$), ***$P < 0.001$, Student's *t*-test. *E*: quantitative analysis of the width of the intercellular spaces between desmosomes in colonic cells of *Villin-Cre* and $Klf5^{\Delta IS}$ mice. Data represent means ± SE ($n = 8$), ***$P < 0.001$, Student's *t*-test.
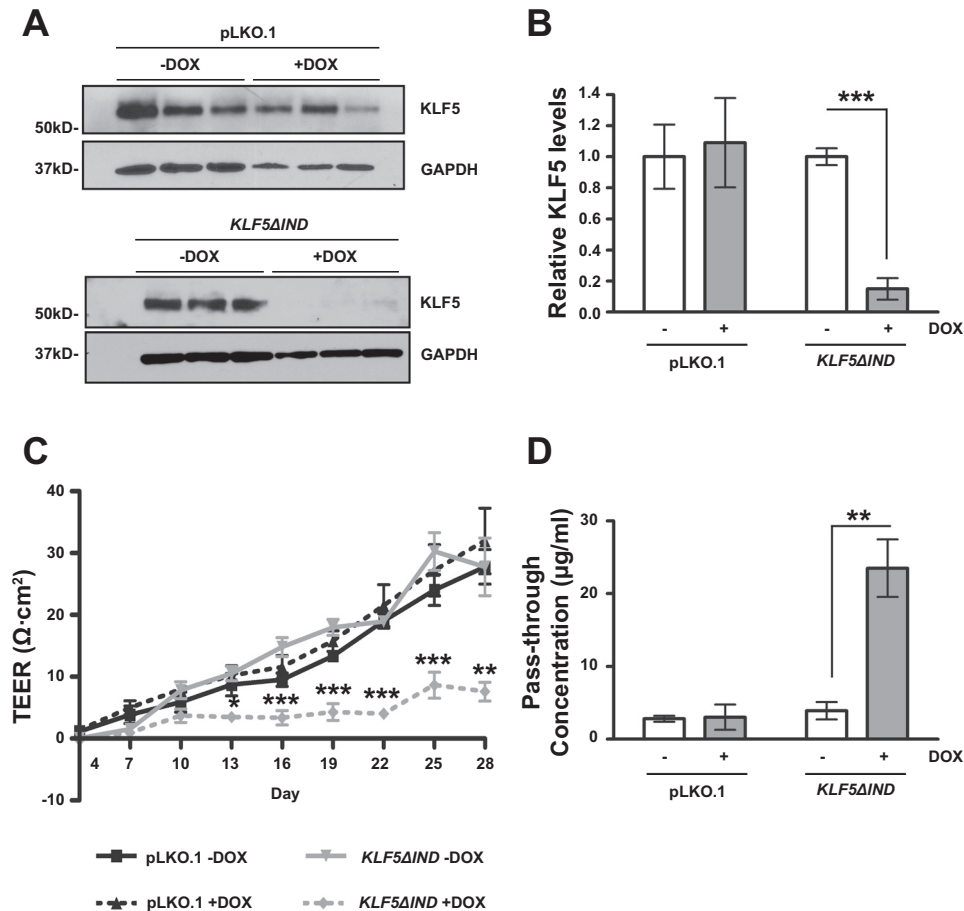
Fig. 3. Epithelial barrier function is impaired in *KLF5* knockdown Caco-2 BBe cells. Caco-2 BBe pLKO.1 cells and Caco-2 BBe *KLF5ΔIND* cells were seeded in Transwell plates. On *day 3* of the culture, cells were treated with water or doxycycline to induce expression of short-hairpin RNA (shRNA). Cells were maintained for a total 28 days. *A*: Western blot analysis of the KLF5 protein levels in Caco-2 BBe *KLF5ΔIND* –DOX and Caco-2 BBe *KLF5ΔIND* +DOX cells (*bottom*) and Caco-2 BBe pLKO.1 –DOX and Caco-2 BBe pLKO.1 +DOX cells (*top*) on *day 28*. A result from 3 independent experiments is shown. *B*: quantitative representation of KLF5 protein levels in 3 independent experiments, normalized to GAPDH. Data represent means ± SE ($n = 3$), ***$P < 0.001$, Student's *t*-test. *C*: transepithelial electrical resistances of Caco-2 BBe *KLF5ΔIND* (gray lines) and Caco-2 BBe wild-type (WT, black lines) monolayers grown in absence (–DOX, solid line) and presence (+DOX, broken line) of doxycycline were measured during 28 days of culture. Data represent means ± SE ($n = 3$), *$P < 0.05$, **$P < 0.01$, and ***$P < 0.001$, Student's *t*-test. *D*: permeability to FITC-4 kDa dextran measured on *day 28*. Data are shown as pass-through concentrations of FITC-dextran. Empty boxes, –DOX; filled boxes, +DOX. Data represent means ± SE ($n = 3$), **$P < 0.01$ by Student's *t*-test.

KLF5ΔIND +DOX cells failed to polarize, and the number of brush-border microvilli on the apical membranes was decreased. Furthermore, the images also indicated that the structures of desmosomes were disrupted in Caco-2 BBe *KLF5ΔIND* +DOX cells, manifested by bulgy desmosome plaques and an enlarged intercellular space between adjacent plasma membranes. We further quantified the number of desmosomes on the basolateral membrane. The average number of desmosomes on each basolateral plasma membrane per section was between five and six in Caco-2 BBe *KLF5ΔIND* –DOX and pLKO.1 –DOX and +DOX cells, whereas the number was decreased to three in Caco-2 BBe *KLF5ΔIND* +DOX cells (Fig. 4*E*). The average width of intercellular gap between desmosome plaques of Caco-2 BBe *KLF5ΔIND* +DOX cells was ~40% wider than that of the control cells (Fig. 4*F*). In contrast, the structure and distribution of apical junctional complexes were maintained upon *KLF5* knockdown. These results suggest that the observed changes in epithelial morphology resulting from KLF5 loss could be attributed to decreased numbers of desmosomes and structural alterations in those present.

DSG2 is required for KLF5-mediated maintenance of epithelial barrier function. To verify that DSG2 plays a role in KLF5-mediated maintenance of the epithelial barrier function, we studied the barrier function of inducible *DSG2* knockdown Caco-2 BBe cells in absence (Caco-2 BBe *DSG2ΔIND* –DOX) or presence (Caco-2 BBe *DSG2ΔIND* +DOX) of doxycycline. Cells were seeded in permeable Transwell plates and grown for

3 days until confluence was achieved, and doxycycline was added on *day 3* and maintained as described in MATERIALS AND METHODS. Western blot analysis of cell lysates collected from the epithelial cell monolayers confirmed a 57% reduction in DSG2 expression in Caco-2 BBe *DSG2ΔIND* +DOX compared with –DOX cells (Fig. 5, *A* and *B*). TEER measurements showed that the establishment of barrier function was significantly impeded in Caco-2 BBe *DSG2ΔIND* +DOX cells compared with the Caco-2 BBe *DSG2ΔIND* –DOX. TEER reached a plateau of 19.0 Ω·cm² on the 28th day of treatment in Caco-2 BBe *DSG2ΔIND* +DOX cells and 71.0 Ω·cm² in the water-treated Caco-2 BBe *DSG2ΔIND* cells (Fig. 5*C*). Consistently, the pass-through concentrations of FITC-4 kDa dextran molecules across the Caco-2 BBe *DSG2ΔIND* +DOX monolayers were approximately ninefold higher than those across the Caco-2 BBe *DSG2ΔIND* –DOX monolayers (Fig. 5*D*). Immunofluorescence staining of DSG2 showed reduced levels and mislocalization of DSG2 in Caco-2 BBe *DSG2ΔIND* +DOX compared with the membranous distribution of DSG2 in Caco-2 BBe *DSG2ΔIND* −DOX cells (Fig. 5*E*, *a* and *b*), verified by quantification of fluorescence intensity (Fig. 5*Ec*). These results demonstrate that *DSG2* knockdown impairs the integrity of barrier function of Caco-2 BBe cells, resulting in increased permeability, as demonstrated in Caco-2 BBe *KLF5ΔIND* +DOX cells.

DSG2 overexpression partially rescues impaired epithelial barrier function caused by KLF5 knockdown. To study whether DSG2 is a major factor that plays a role in KLF5-
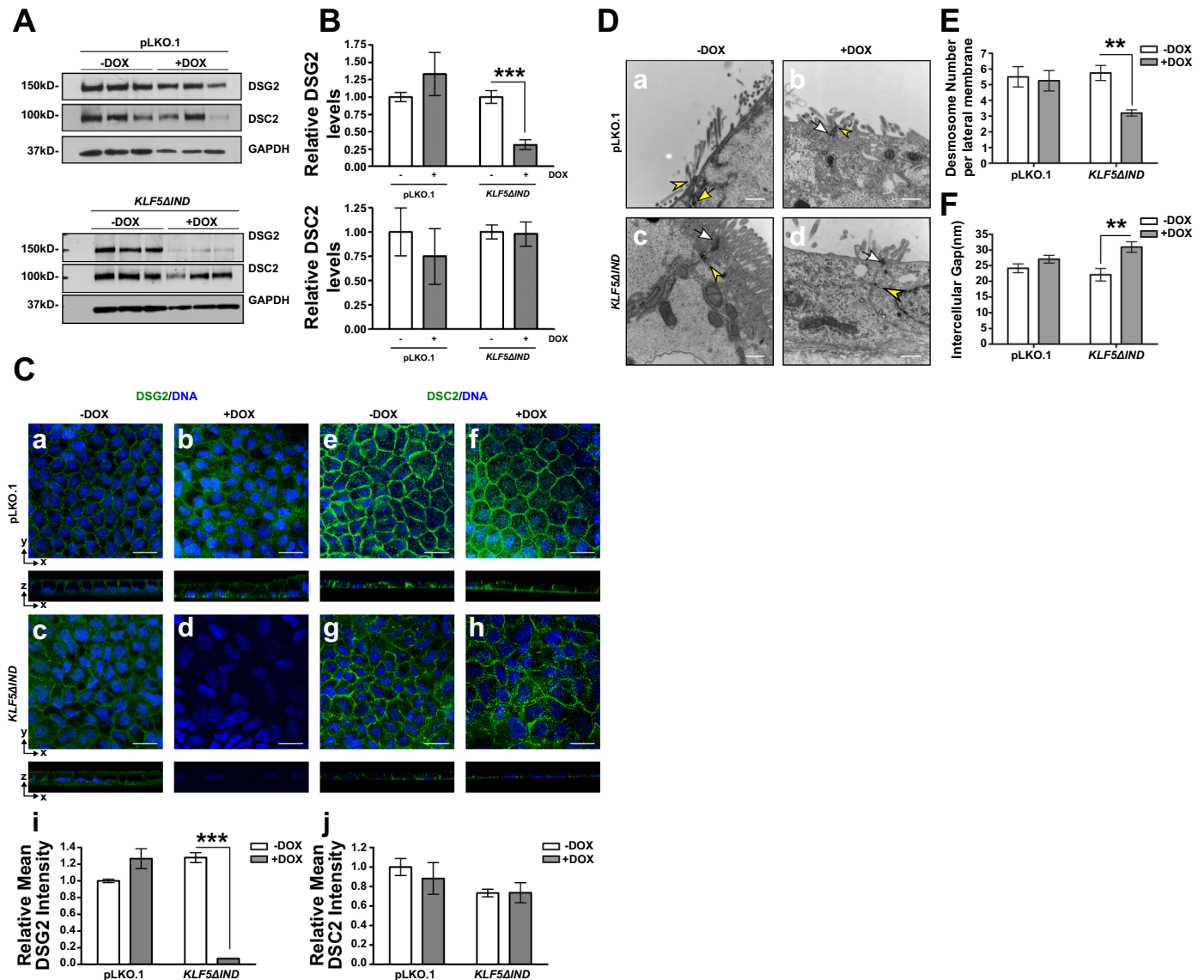
Fig. 4. Expression of DSG2 but not DSC2 is reduced and desmosomal morphology is changed upon *KLF5* knockdown in Caco-2 BBe cells. Caco-2 BBe pLKO.1 and *KLF5ΔIND* cells were seeded in Transwell plates, and, on *day 3* of the culture, cells were treated with water or doxycycline to induce expression of shRNA. *A*: Western blot analysis of the DSG2 and DSC2 protein levels in Caco-2 BBe pLKO.1 −DOX and +DOX and Caco-2 Bbe *KLF5ΔIND* −DOX and +DOX cells (*bottom*) on *day 28*. A result from 3 independent experiments is shown. *B*: quantitative representation of DSG2 and DSC2 protein levels in 3 independent experiments, normalized to GAPDH. Data represent means ± SE ($n = 3$), ***$P < 0.001$, Student's *t*-test. *C*: immunofluorescence staining of DSG2 (*a–d*) and DSC2 (*e–h*) in Caco-2 BBe pLKO.1 −DOX/+DOX and Caco-2 BBe *KLF5ΔIND* −DOX/+DOX cells collected on *day 28* of culture. The *top* part of each panel shows *X–Y* projections obtained from Z-stacks, and companion Z-plane cross sections are shown on *bottom*. DNA was counterstained with TO-PRO3. Images were taken at ×400 magnification. Scale bars indicate 20 μm. Relative mean fluorescence intensity was quantified (*i* and *j*). Data represent means ± SE ($n = 6$), ***$P < 0.001$ by Student's *t*-test. *D*: transmission electron microscopy images showing different morphologies involving decreased microvilli numbers and altered desmosome structures between Caco-2 BBe pLKO.1 −DOX/+DOX, Caco-2 BBe *KLF5ΔIND* −DOX (*a–c*, ×30,000 magnification), and Caco-2 BBe *KLF5ΔIND* +DOX cells (*d*, ×30,000 magnification). White arrows, apical junctional complexes; yellow arrowheads, desmosomes. Scale bars indicate 400 nm. *E*: quantitative analysis of the number of desmosomes in Caco-2 BBe pLKO.1 −DOX/+DOX, Caco-2 BBe *KLF5ΔIND* −DOX, and Caco-2 BBe *KLF5ΔIND* +DOX cells. Data represent means ± SE ($n = 4$ for pLKO.1 −DOX, $n = 8$ for pLKO.1 +DOX, $n = 4$ for Caco-2 BBe *KLF5ΔIND* −DOX, and $n = 5$ for Caco-2 BBe *KLF5ΔIND* +DOX), **$P < 0.01$, Student's *t*-test. *F*: quantitative analysis of the width of the intercellular spaces between desmosomes in Caco-2 BBe *KLF5ΔIND* −DOX and Caco-2 BBe *KLF5ΔIND* +DOX cells. Data represent means ± SE ($n = 26$ for pLKO.1 −DOX, $n = 42$ for pLKO.1 +DOX, $n = 12$ for Caco-2 BBe *KLF5ΔIND* −DOX, and $n = 8$ for Caco-2 BBe *KLF5ΔIND* +DOX), **$P < 0.01$, Student's *t*-test.

mediated maintenance of epithelial barrier function, we studied the barrier function of *DSG2*-overexpressing Caco-2 BBe *KLF5ΔIND* cells in the absence (Caco-2 BBe *KLF5ΔIND DSG2* −DOX) or presence (Caco-2 BBe *KLF5ΔIND DSG2* +DOX) of doxycycline, along with the control cell line in the absence (Caco-2 BBe *KLF5ΔIND EV* −DOX) or presence (Caco-2 BBe *KLF5ΔIND EV* +DOX) of doxycycline. Cells

were seeded in permeable Transwell plates and grown for 3 days until confluence was achieved, and doxycycline was added on *day 3* and maintained as described in MATERIALS AND METHODS. The TEER reached the maximum value on *day 55* postseeding. TEER measurements during the time period of 55 days showed that the establishment of barrier function was significantly impeded in Caco-2 BBe *KLF5ΔIND EV* +DOX
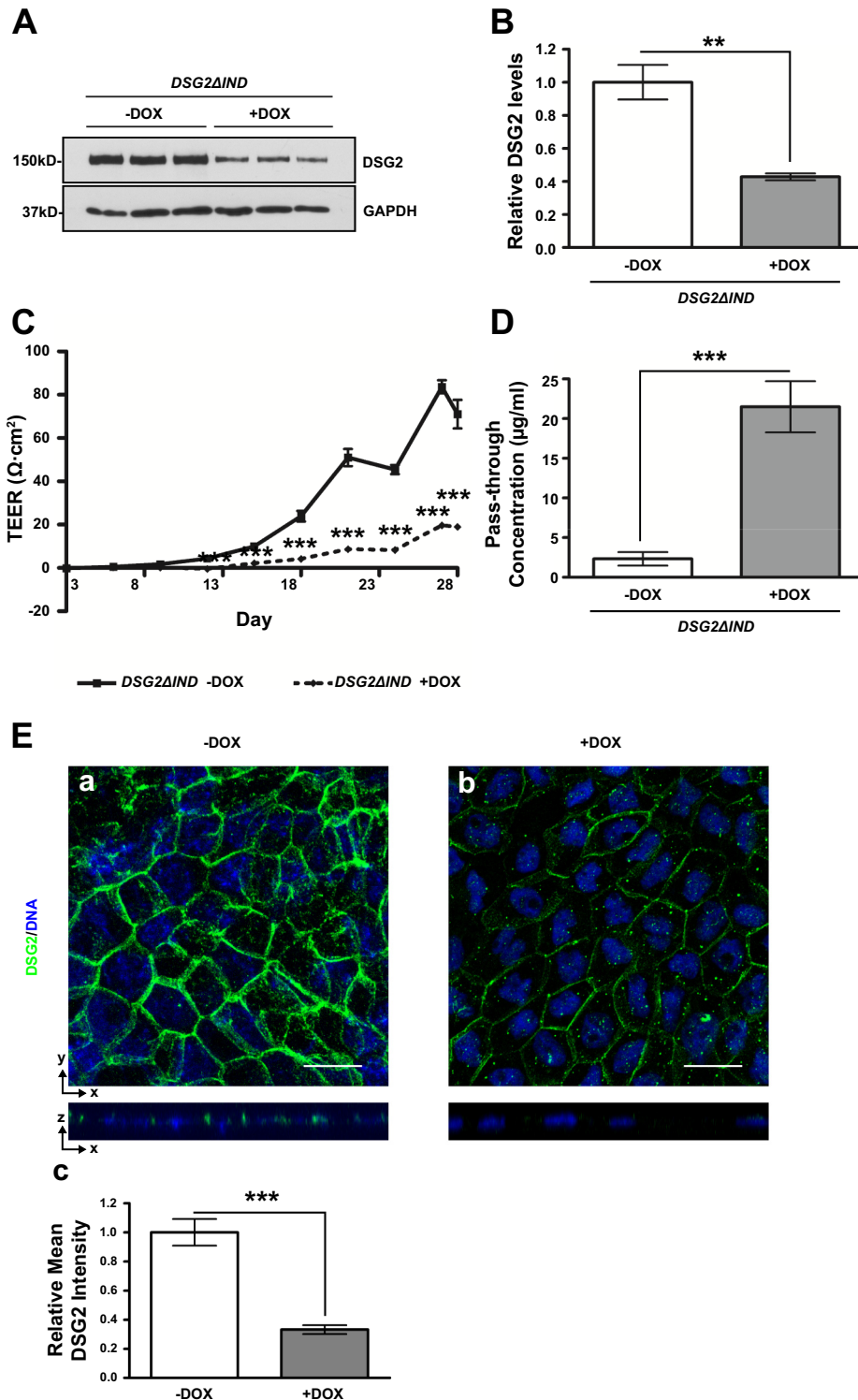
A

B

C

D

E

Fig. 5. Epithelial barrier function is impaired in *DSG2* knockdown Caco-2 BBe cells. Caco-2 BBe *DSG2ΔIND* cells were seeded in Transwell plates. On *day 3* of the culture, cells were treated with water or doxycycline to induce expression of shRNA. Cells were maintained for a total of 28 days. *A*: Western blot analysis of the DSG2 protein levels in Caco-2 BBe *DSG2ΔIND* –DOX and Caco-2 BBe *DSG2ΔIND* +DOX cells (*bottom*) on *day 28*. A result from 3 independent experiments is shown. *B*: quantitative representation of DSG2 protein levels in 3 independent experiments, normalized to GAPDH. Data represent means ± SE ($n = 3$), **$P < 0.01$, Student's *t*-test. *C*: transepithelial electrical resistances of Caco-2 BBe *DSG2ΔIND* monolayers grown in absence (–DOX, solid line) and presence (+DOX, broken line) of doxycycline were measured during 28 days of culture. Data represent means ± SE ($n = 6$), ***$P < 0.001$, Student's *t*-test. *D*: permeability to FITC-4 kDa dextran measured on *day 28*. Data are shown as pass-through concentrations of FITC-dextran. Empty boxes, –DOX; filled boxes, +DOX. Data represent means ± SE ($n = 6$), ***$P < 0.001$ by Student's *t*-test. *E*: immunofluorescence staining of DSG2 in Caco-2 BBe *DSG2ΔIND* –DOX and Caco-2 BBe *DSG2ΔIND* +DOX cells collected on *day 28* of culture. The *top* part of each panel shows *X–Y* projections obtained from Z-stacks, and companion Z-plane cross sections are shown on *bottom*. DNA was counterstained with TO-PRO3. Images were taken at ×400 magnification. Scale bars indicate 20 μm. Relative mean fluorescence intensity was quantified (*c*). Data represent means ± SE ($n = 6$), ***$P < 0.001$ by Student's *t*-test.

cells compared with Caco-2 BBe *KLF5ΔIND EV* –DOX. *DSG2* overexpression enhanced barrier function in Caco-2 BBe *KLF5ΔIND DSG2* –DOX and partially rescued the impaired barrier function in Caco-2 BBe *KLF5ΔIND DSG2* +DOX. TEER reached a plateau of 47.7 Ω·cm² on the 55th day of treatment in Caco-2 BBe *KLF5ΔIND EV* –DOX cells, 6.8 Ω·cm² in Caco-2 BBe *KLF5ΔIND EV* +DOX cells, 69.2 Ω·cm² in Caco-2 BBe *KLF5ΔIND DSG2* –DOX cells, and 18.0

Ω·cm² in Caco-2 BBe *KLF5ΔIND DSG2* +DOX cells (Fig. 6*A*). Consistently, the pass-through concentrations of FITC-4 kDa dextran molecules across the Caco-2 BBe *KLF5ΔIND DSG2* +DOX monolayers were approximately sevenfold higher than those across the Caco-2 BBe *KLF5ΔIND DSG2* –DOX monolayers, in contrast to the ninefold increase in Caco-2 BBe *KLF5ΔIND EV* +DOX compared with Caco-2 BBe *KLF5ΔIND EV* –DOX (Fig. 6*B*). Immunofluorescence

Fig. 6. Overexpression of DSG2 partially rescues impaired barrier function upon *KLF5* knockdown in Caco-2 BBe cells. Caco-2 BBe *KLF5ΔIND EV* and *KLF5ΔIND DSG2* cells were seeded in Transwell plates, and, on *day 3* of the culture, cells were treated with water or doxycycline to induce expression of shRNA. Cells were maintained for a total 55 days. *A*: transepithelial electrical resistances of Caco-2 BBe *KLF5ΔIND EV* (black lines) and Caco-2 BBe *KLF5ΔIND DSG2* (gray lines) monolayers grown in absence (–DOX, solid line) and presence (+DOX, broken line) of doxycycline were measured during 55 days of culture. Data represent means ± SE (*n* = 3), **P* < 0.05 and ****P* < 0.001, Student's *t*-test. *B*: permeability to FITC-4 kDa dextran measured on *day 55*. Data are shown as pass-through concentrations of FITC-dextran. Empty boxes, –DOX; filled boxes, +DOX. Data represent means ± SE (*n* = 3), ***P* < 0.01 and ****P* < 0.001 by Student's *t*-test. *C*: immunofluorescence staining of DSG2 in Caco-2 BBe *KLF5ΔIND EV* –DOX (*a*)/+DOX (*b*) and Caco-2 BBe *KLF5ΔIND DSG2* –DOX (*c*)/+DOX (*d*) cells collected on *day 55* of culture. The *top* part of each panel shows *X–Y* projections obtained from Z-stacks, and companion Z-plane cross sections are shown on *bottom*. DNA was counterstained with TO-PRO3. Images were taken at ×400 magnification. Scale bars indicate 20 μm. Relative mean fluorescence intensity was quantified (*e*). Data represent means ± SE (*n* = 6), **P* < 0.05 and ****P* < 0.001 by Student's *t*-test.
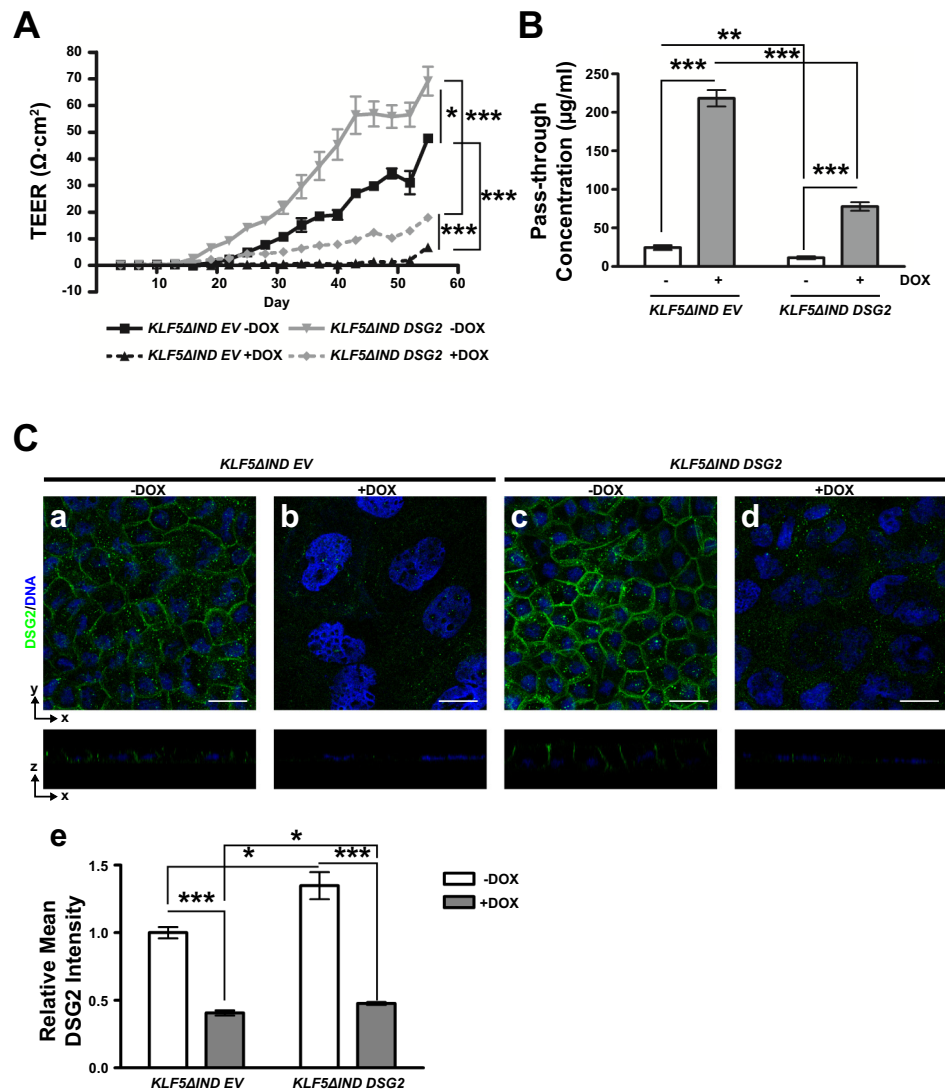
staining of DSG2 showed reduced levels and mislocalization of DSG2 in Caco-2 BBe *KLF5ΔIND EV* +DOX (Fig. 6*Cb*) compared with the membranous distribution of DSG2 in Caco-2 BBe *KLF5ΔIND EV* –DOX cells (Fig. 6*Ca*), and slightly increased level of DSG2 by 30% in Caco-2 BBe *KLF5ΔIND DSG2* –DOX cells (Fig. 6*Ce*), accompanied with a thick monolayer of mature columnar epithelial cells (Fig. 6*Cc*). DSG2 was partially restored by 10% on cell membranes in Caco-2 BBe *KLF5ΔIND DSG2* +DOX cells (Fig. 6*C, d* and *e*). These results demonstrate that *DSG2* overexpression partially rescues the barrier function of Caco-2 BBe cells upon *KLF5* knockdown and increases the epithelial barrier function of Caco-2 BBe on a basal level.

KLF5 regulates DSG2 promoter activity. Potential KLF5-binding sites were identified with the KLF5-binding motifs identified in a previous study (28) (Fig. 7*A*), and ChIP study showed that KLF5 interacts with all of the promoter sequences that cover the potential KLF5-binding sites (Fig. 7*B*). Mutations were introduced in respective KLF5-binding sites, and the sequences are listed in Fig. 7*B*. Because of the endogenous *KLF5* expression in HEK 293T cells, *DSG2* promoter has a high basal level activity. Mutant *DSG2* promoter MUT1 has a

similar basal level as the wild-type *DSG2* promoter, but KLF5 overexpression failed to enhance the promoter activity; MUT2 and MUT3 showed decreased basal levels of promoter activities, and the KLF5-mediated transactivation of *DSG2* promoter was partially impaired (Fig. 7*C*). These results indicated a direct interaction of KLF5 and *DSG2* promoter at multiple binding sites, and *site 1* is crucial for KLF5-mediated transactivation of *DSG2* promoter.

DISCUSSION

KLF5 is highly expressed in the proliferative compartment of small intestine and colon, and previous studies from our laboratory demonstrated that KLF5 is required for the maintenance of the crypt architecture and barrier function in the mouse intestine (22). Herein we investigated the mechanisms by which KLF5 regulates colonic barrier function.

We have previously shown that inducible intestine-specific deletion of *Klf5* in adult mice caused signs of epithelial distress in colonic tissues (26). In colonic tissues collected from the corn oil- or tamoxifen-injected 8-wk-old adult female *Klf5ΔIND* mice and the 5-wk-old adult *Villin-Cre* and *Klf5ΔIS* mice, a

A

```
-500 TTGGTCCGCGCAGGACTCTGCTCCGTGGAGCTTTTGTCCTTGGGCCGGGGCCCTGCGACCCGCGCTACCCAGGTCGAGCCC
           Site 1                                                              Site 2
-420 CGCCAGGAGGCTCCCTCCTCCCGCCATTCTCCAGAGAGTAGGGGGTCGGGAAGGAGAGAACGGCGGGGCGGGGCCTGCCA
        Site 3
-340 CCCACAGTCCCCAACCCAAGGACGTCACGGTCCCAGGTGCGAGTGCGAGCGGGCGGGAGTCCACCCCGCGCCTCCCTCCT
-260 CTGCTGAACTCCCCACCTCTGTAAAAGCGGCCCGGGCCGGCCCCCGGCTCCATTTTCTCGCGGCGGCCACACCTGGAGCC
-180 GCGCCTTTGGGTTGGGCTGGGCTGGGCCGCGCAACCGCCACGGGAAGACAGCCCTCGGGGCGGGGAGGGAGAGGGTGGCC
-100 GGGCCGGGGGGAGGCCGGGGCCAGGGAGGAGCCGAGTGCGCGCTCGGGGCAGGCGGCGGCGCGGAGCGGTGCGGCGGCGG
 -20 GAGGCGGAGGCGAGGGTGCGATG
```

B

Site 1
Site 2&3

Mutant 1: CCGCAGGAC → ACATAGTAC
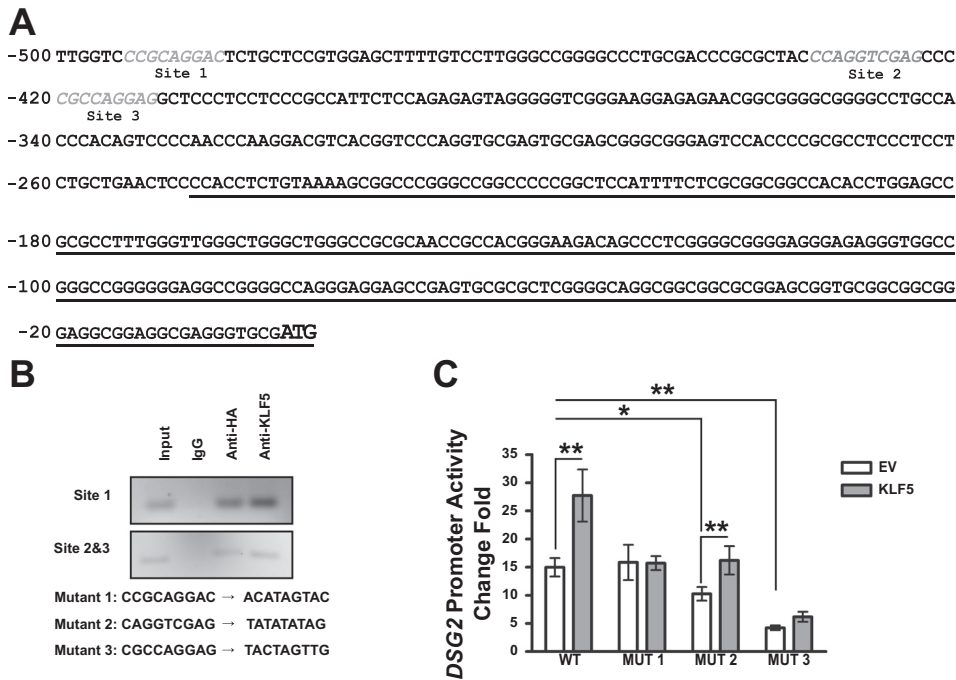Mutant 2: CAGGTCGAG → TATATATAG
Mutant 3: CGCCAGGAG → TACTAGTTG

C

Fig. 7. KLF5-binding sites are identified in *DSG2* promoter. *A*: sequences of the potential binding sites for KLF5 are shown in gray and italic within 500 bp upstream of the start codon of *DSG2*, with transcript underlined. *B*: PCR products of *DSG2* promoter sequences in input cell lysates and immunoprecipitations with rabbit IgG, rabbit HA antibody, and KLF5 antibody using HEK 293T cells cotransfected with pGL3BDSG2(500) and pMT3-HA-KLF5. Sequences of the site-directed mutation of the binding sites are shown. *C*: *DSG2* promoter activity measured with luciferase assay. HEK 293T cells were transfected pEGFP-ΔEGFP or pEGFP-ΔEGFP-KLF5-HA together with pLightSwitch, pLightSwitch-DSG2(500), or pLightSwitch-DSG2(500) mutant promoter reporter plasmids. Data represent means ± SE ($n = 18$), *$P < 0.05$ and **$P < 0.01$ by Student's *t*-test.

correlation of KLF5 and DSG2 is discovered. KLF5 and DSG2 are highly expressed in human colon cancer tissues (39), and DSG2 levels in the KLF5-positive crypts in $Klf5^{\Delta IS}$ tissues resulting from variegated *Klf5* knockout are higher than that in *Klf5*-depleted crypts (data not shown); thus, it is likely that KLF5 and DSG2 levels have a direct positive correlation. The KLF5-dependent expression of DSG2 could explain the findings of many studies that addressed their physiological functions, ranging from embryonic development to inflammatory bowel diseases and tumorigenesis. $Dsg2^{-/-}$ mouse embryos and some $Dsg2^{+/-}$ embryos died at the blastocyst stage of embryonic development because of defective implantation (8). Moreover, embryonal stem cells derived from $Dsg2^{-/-}$ embryos were eliminated by *day 6* in culture, indicating that DSG2 is essential for embryonal stem cell growth (8). Importantly, similar phenotypes were reported for $Klf5^{-/-}$ mouse embryos (29). Another genome-wide ChIP and microarray study on *Klf5* knockdown in embryonic stem cells showed that expression of *Dsg2* is downregulated upon *siKlf5* transfection (28). These results suggest potential overlapping functions of KLF5 and DSG2 in the development of mouse embryonic stem cells. Additionally, loss of both DSG2 and DSC2 in SK-CO15 cells has been studied and indicated that reduced DSG2 level inhibits cell proliferation via epidermal growth factor receptor signaling (13), which aligns with the proproliferative effect of KLF5 on intestinal epithelial cells harboring activated *KRAS* mutation (24). Furthermore, our preliminary results from short-term experiments show that deletion of *DSG2* in Caco2 cells decreases, however not significantly, proliferation of these cells compared with control (data not shown). Studies have also demonstrated a decrease in both *KLF5* and *DSG2* expression in colonic tissues from patients with inflammatory bowel disease (35, 43). These results support the hypothesis that loss of KLF5 in the intestinal epithelium can result in decrease of DSG2 expression and lead to loss of barrier function and inflammation that are the hallmark of inflammatory conditions,

e.g., in Crohn's disease. Our data demonstrate that the basal expression levels of the desmosomal cadherins *Dsg1*, *-3*, and *-4* and *Dsc1* and *-3* are undetectable in control and $Klf5^{\Delta IS}$ mouse animal models, and cytokeratin-8 and *-18*, components of intermediate filament, are not changed upon *Klf5* deletion (data not shown). mRNA levels of other cell junction components such as E-cadherin, α-catenin, β-catenin, ZO-1, occludin, JAM-A, claudin-2, claudin-4, and claudin-12 were not primarily changed by *Klf5* knockout.

Previous studies from our laboratory showed that KLF5 promotes proliferation of cultured cells (24). To minimize the potential effects of slowed cell proliferation caused by *KLF5* knockdown, we used the inducible *KLF5* knockdown cell line and did not induce knockdown until cells had reached confluence, between *days 3* and *4* after seeding. Therefore, it is unlikely that the impaired barrier function is merely because of KLF5′s effect on cell proliferation. Our evidence strongly suggests that the effect of KLF5 on barrier function is because of its regulation of cell junctions and subsequent changes in epithelial morphology.

We showed a correlation of DSG2 and KLF5 levels in the Caco-2 BBe cell line, consistent with our in vivo observations. Several studies have demonstrated that DSG2 is essential for maintaining the integrity of intestinal epithelial barrier. For example, a DSG2 antibody that detects the extracellular domain specifically blocks DSG2 interaction in the cell-free system and significantly increases epithelial permeability of Caco-2 cells (31). IL-10-mediated enhancement of the epithelial barrier in the presence of corticosteroids is also accompanied by an increase in DSG2 expression, whereas its expression is reduced in colonic epithelial cells of glucocorticoid-refractory patients (19). A study on human ulcerative colitis and Crohn's disease patient tissues showed that the distribution and intensity of DSG2 staining were not strikingly different in noninflamed tissues from that seen in control tissue but were significantly reduced in inflamed mucosal tissues (35). Our

results also confirmed the role of DSG2 in barrier function by knocking down *DSG2* in Caco-2 BBe cells. However, overexpression of DSG2 could not completely rescue the impaired barrier function in *KLF5* knockdown Caco-2 BBe cells, suggesting that DSG2 might not be the only factor that KLF5 affects to maintain barrier function. Additionally, we analyzed the mRNA levels of several tight/adherent junction proteins (*TJP1*, *OCLN*, *CLDN4*, and *CDH1*) in *DSG2* knockdown cells but did not observe any significant decrease (data not shown). Taken together, these results indicate that DSG2 exerts an important role in regulating intestinal barrier function.

Because DSG2 was significantly decreased in Caco-2 BBe *KLF5ΔIND* +DOX cells, DSG2 may be an effector of KLF5-mediated epithelial barrier function. Loss of DSG2 is accompanied by altered desmosome structures and number. Many studies on desmosomes reported that desmosome assembly is sensitive to isoform-specific differences exhibited by desmosomal cadherins and that desmogleins and desmocollins interact in a heterophilic manner in mature desmosomes (6, 20). Although DSC2 can compensate for the loss of DSG2 from desmosomes to some extent in the colon cancer cell line SK-CO15 (13), the expression and distribution of DSC2 is not changed by *KLF5* knockdown in our Caco-2 BBe cell system and *Klf5ΔIS* mouse model. The reduction of DSC2 levels in tamoxifen-induced *Klf5ΔIND* mice could be because of a secondary response to the loss of DSG2 from the DSG2-DSC2 heterodimers, whereas DSC2 can be stabilized in DSC2 homodimers that might be a major form of desmosomal cadherin dimers in *Klf5ΔIS* mouse tissues to compensate for the loss of DSG2. The other possible reason goes to the fact that the adult *Klf5ΔIS* mice used for experiments were survivors who had partial expression of KLF5. Functional studies on models of *DSG2* knockdown further substantiated the effector role of DSG2 in KLF5-mediated establishment of epithelial barrier function.

Because of its transcription role, a majority of studies on KLF5 are focused on transcription regulation of potential KLF5 target genes. Having screened the KLF5-binding motifs identified in a study that combined genome-wide ChIP and microarray analysis (28), we identified three KLF5-binding motifs within the 500-bp region of *DSG2* promoter compared with none within *HPRT1* promoter. Consistently, our ChIP results and promoter study showed a positive effect of KLF5 in activating the *DSG2* promoter, indicating that KLF5 regulates DSG2 expression by serving as a direct transcription activator of the *DSG2* gene. The unexpected unchanged basal level of *DSG2* promoter mutant at site 1 can be the result of the potential transactivation by other transcription factors. Because the promoter activity of mutant at site 1 was not enhanced by *KLF5* overexpression, site 1 could be the major binding site for KLF5; sites 2 and 3 are in tandem, and mutation on one of them just partially depleted *DSG2* promoter KLF5-mediated transactivation; thus, these two sites might work in combination for KLF5 binding.

REFERENCES

1. **Bell SM, Zhang L, Mendell A, Xu Y, Haitchi HM, Lessard JL, Whitsett JA.** Kruppel-like factor 5 is required for formation and differentiation of the bladder urothelium. *Dev Biol* 358: 79–90, 2011. doi:10.1016/j.ydbio.2011.07.020.

2. **Bell SM, Zhang L, Xu Y, Besnard V, Wert SE, Shroyer N, Whitsett JA.** Kruppel-like factor 5 controls villus formation and initiation of cytodifferentiation in the embryonic intestinal epithelium. *Dev Biol* 375: 128–139, 2013. doi:10.1016/j.ydbio.2012.12.010.

3. **Chen C, Benjamin MS, Sun X, Otto KB, Guo P, Dong X-Y, Bao Y, Zhou Z, Cheng X, Simons JW, Dong J-T.** KLF5 promotes cell proliferation and tumorigenesis through gene regulation and the TSU-Pr1 human bladder cancer cell line. *Int J Cancer* 118: 1346–1355, 2006. doi:10.1002/ijc.21533.

4. **Chen C, Bhalala HV, Qiao H, Dong J-T.** A possible tumor suppressor role of the KLF5 transcription factor in human breast cancer. *Oncogene* 21: 6567–6572, 2002. doi:10.1038/sj.onc.1205817.

5. **Chen C, Bhalala HV, Vessella RL, Dong J-T.** KLF5 is frequently deleted and down-regulated but rarely mutated in prostate cancer. *Prostate* 55: 81–88, 2003. doi:10.1002/pros.10205.

6. **Chitaev NA, Troyanovsky SM.** Direct Ca2+-dependent heterophilic interaction between desmosomal cadherins, desmoglein and desmocollin, contributes to cell-cell adhesion. *J Cell Biol* 138: 193–201, 1997. doi:10.1083/jcb.138.1.193.

7. **Clayburgh DR, Shen L, Turner JR.** A porous defense: the leaky epithelial barrier in intestinal disease. *Lab Invest* 84: 282–291, 2004. doi:10.1038/labinvest.3700050.

8. **Eshkind L, Tian Q, Schmidt A, Franke WW, Windoffer R, Leube RE.** Loss of desmoglein 2 suggests essential functions for early embryonic development and proliferation of embryonic stem cells. *Eur J Cell Biol* 81: 592–598, 2002. doi:10.1078/0171-9335-00278.

9. **Farquhar MG, Palade GE.** Junctional complexes in various epithelia. *J Cell Biol* 17: 375–412, 1963. doi:10.1083/jcb.17.2.375.

10. **Groschwitz KR, Hogan SP.** Intestinal barrier function: molecular regulation and disease pathogenesis. *J Allergy Clin Immunol* 124: 3–20, 2009. doi:10.1016/j.jaci.2009.05.038.

11. **Hermiston ML, Gordon JI.** In vivo analysis of cadherin function in the mouse intestinal epithelium: essential roles in adhesion, maintenance of differentiation, and regulation of programmed cell death. *J Cell Biol* 129: 489–506, 1995. doi:10.1083/jcb.129.2.489.

12. **Ivanov AI, Parkos CA, Nusrat A.** Cytoskeletal regulation of epithelial barrier function during inflammation. *Am J Pathol* 177: 512–524, 2010. doi:10.2353/ajpath.2010.100168.

13. **Kamekura R, Kolegraff KN, Nava P, Hilgarth RS, Feng M, Parkos CA, Nusrat A.** Loss of the desmosomal cadherin desmoglein-2 suppresses colon cancer cell proliferation through EGFR signaling. *Oncogene* 33: 4531–4536, 2014. doi:10.1038/onc.2013.442.

14. **Kamekura R, Nava P, Feng M, Quiros M, Nishio H, Weber DA, Parkos CA, Nusrat A.** Inflammation-induced desmoglein-2 ectodomain shedding compromises the mucosal barrier. *Mol Biol Cell* 26: 3165–3177, 2015. doi:10.1091/mbc.E15-03-0147.

15. **Kenchegowda D, Swamynathan S, Gupta D, Wan H, Whitsett J, Swamynathan SK.** Conditional disruption of mouse Klf5 results in defective eyelids with malformed meibomian glands, abnormal cornea and loss of conjunctival goblet cells. *Dev Biol* 356: 5–18, 2011. doi:10.1016/j.ydbio.2011.05.005.

16. **Kutner RH, Zhang X-Y, Reiser J.** Production, concentration and titration of pseudotyped HIV-1-based lentiviral vectors. *Nat Protoc* 4: 495–505, 2009. doi:10.1038/nprot.2009.22.

17. **Laukoetter MG, Nava P, Nusrat A.** Role of the intestinal barrier in inflammatory bowel disease. *World J Gastroenterol* 14: 401–407, 2008. doi:10.3748/wjg.14.401.

18. **Li Q, Dong Z, Zhou F, Cai X, Gao Y, Wang LW.** Krüppel-like factor 5 promotes lung tumorigenesis through upregulation of Sox4. *Cell Physiol Biochem* 33: 1–10, 2014. doi:10.1159/000356645.

19. **Lorén V, Cabré E, Ojanguren I, Domènech E, Pedrosa E, García-Jaraquemada A, Mañosa M, Manyé J.** Interleukin-10 enhances the intestinal epithelial barrier in the presence of corticosteroids through p38 MAPK activity in Caco-2 monolayers: a possible mechanism for steroid responsiveness in ulcerative colitis. *PLoS One* 10: e0130921, 2015. doi:10.1371/journal.pone.0130921.

20. **Lowndes M, Rakshit S, Shafraz O, Borghi N, Harmon RM, Green KJ, Sivasankar S, Nelson WJ.** Different roles of cadherins in the assembly and structural integrity of the desmosome complex. *J Cell Sci* 127: 2339–2350, 2014. doi:10.1242/jcs.146316.

21. **Marcozzi C, Burdett ID, Buxton RS, Magee AI.** Coexpression of both types of desmosomal cadherin and plakoglobin confers strong intercellular adhesion. *J Cell Sci* 111: 495–509, 1998.

22. **McConnell BB, Kim SS, Yu K, Ghaleb AM, Takeda N, Manabe I, Nusrat A, Nagai R, Yang VW.** Krüppel-like factor 5 is important for maintenance of crypt architecture and barrier function in mouse intestine. *Gastroenterology* 141: 1302–1313, 2011. doi:10.1053/j.gastro.2011.06.086.

23. **Mir H, Meena AS, Chaudhry KK, Shukla PK, Gangwar R, Manda B, Padala MK, Shen L, Turner JR, Dietrich P, Dragatsis I, Rao R.** Occludin deficiency promotes ethanol-induced disruption of colonic epithelial junctions, gut barrier dysfunction and liver damage in mice. *Biochim Biophys Acta* 1860: 765–774, 2016. doi:10.1016/j.bbagen.2015.12.013.

24. **Nandan MO, Chanchevalap S, Dalton WB, Yang VW.** Krüppel-like factor 5 promotes mitosis by activating the cyclin B1/Cdc2 complex during oncogenic Ras-mediated transformation. *FEBS Lett* 579: 4757–4762, 2005. doi:10.1016/j.febslet.2005.07.053.

25. **Nandan MO, Ghaleb AM, Bialkowska AB, Yang VW.** Krüppel-like factor 5 is essential for proliferation and survival of mouse intestinal epithelial stem cells. *Stem Cell Res (Amst)* 14: 10–19, 2015. doi:10.1016/j.scr.2014.10.008.

26. **Nandan MO, Ghaleb AM, Liu Y, Bialkowska AB, McConnell BB, Shroyer KR, Robine S, Yang VW.** Inducible intestine-specific deletion of Krüppel-like factor 5 is characterized by a regenerative response in adult mouse colon. *Dev Biol* 387: 191–202, 2014. doi:10.1016/j.ydbio.2014.01.002.

27. **Nandan MO, McConnell BB, Ghaleb AM, Bialkowska AB, Sheng H, Shao J, Babbin BA, Robine S, Yang VW.** Krüppel-like factor 5 mediates cellular transformation during oncogenic KRAS-induced intestinal tumorigenesis. *Gastroenterology* 134: 120–130, 2008. doi:10.1053/j.gastro.2007.10.023.

28. **Parisi S, Cozzuto L, Tarantino C, Passaro F, Ciriello S, Aloia L, Antonini D, De Simone V, Pastore L, Russo T.** Direct targets of Klf5 transcription factor contribute to the maintenance of mouse embryonic stem cell undifferentiated state. *BMC Biol* 8: 128, 2010. doi:10.1186/1741-7007-8-128.

29. **Parisi S, Passaro F, Aloia L, Manabe I, Nagai R, Pastore L, Russo T.** Klf5 is involved in self-renewal of mouse embryonic stem cells. *J Cell Sci* 121: 2629–2634, 2008. doi:10.1242/jcs.027599.

30. **Schäfer S, Stumpp S, Franke WW.** Immunological identification and characterization of the desmosomal cadherin Dsg2 in coupled and uncou-pled epithelial cells and in human tissues. *Differentiation* 60: 99–108, 1996. doi:10.1046/j.1432-0436.1996.6020099.x.

31. **Schlegel N, Meir M, Heupel W-M, Holthöfer B, Leube RE, Waschke J.** Desmoglein 2-mediated adhesion is required for intestinal epithelial barrier integrity. *Am J Physiol Gastrointest Liver Physiol* 298: G774–G783, 2010. doi:10.1152/ajpgi.00239.2009.

32. **Schmittgen TD, Livak KJ.** Analyzing real-time PCR data by the comparative C(T) method. *Nat Protoc* 3: 1101–1108, 2008. doi:10.1038/nprot.2008.73.

33. **Schneider CA, Rasband WS, Eliceiri KW.** NIH Image to ImageJ: 25 years of image analysis. *Nat Methods* 9: 671–675, 2012. doi:10.1038/nmeth.2089.

34. **Shao Y, Wolf PG, Guo S, Guo Y, Gaskins HR, Zhang B.** Zinc enhances intestinal epithelial barrier function through the PI3K/AKT/mTOR signaling pathway in Caco-2 cells. *J Nutr Biochem* 43: 18–26, 2017. doi:10.1016/j.jnutbio.2017.01.013.

35. **Spindler V, Meir M, Vigh B, Flemming S, Hütz K, Germer C-T, Waschke J, Schlegel N.** Loss of desmoglein 2 contributes to the pathogenesis of Crohn's Disease. *Inflamm Bowel Dis* 21: 2349–2359, 2015. doi:10.1097/MIB.0000000000000486.

36. **Staehelin LA.** Three types of gap junctions interconnecting intestinal epithelial cells visualized by freeze-etching. *Proc Natl Acad Sci USA* 69: 1318–1321, 1972. doi:10.1073/pnas.69.5.1318.

37. **Stefania Vetrano MR, Cera MR, Correale C, Rumio C, Doni A, Fantini M, Sturm A, Borroni E, Repici A, Locati M, Malesci A, Dejana E, Danese S.** Unique role of junctional adhesion molecule-a in maintaining mucosal homeostasis in inflammatory bowel disease. *Gastroenterology* 135: 173–184, 2008. doi:10.1053/j.gastro.2008.04.002.

38. **Tetreault M-P, Alrabaa R, McGeehan M, Katz JP.** Krüppel-like factor 5 protects against murine colitis and activates JAK-STAT signaling in vivo. *PLoS One* 7: e38338, 2012. doi:10.1371/journal.pone.0038338.

39. **Uhlén M, Fagerberg L, Hallström BM, Lindskog C, Oksvold P, Mardinoglu A, Sivertsson Å, Kampf C, Sjöstedt E, Asplund A, Olsson I, Edlund K, Lundberg E, Navani S, Szigyarto CA-K, Odeberg J, Djureinovic D, Takanen JO, Hober S, Alm T, Edqvist P-H, Berling H, Tegel H, Mulder J, Rockberg J, Nilsson P, Schwenk JM, Hamsten M, von Feilitzen K, Forsberg M, Persson L, Johansson F, Zwahlen M, von Heijne G, Nielsen J, Pontén F.** Proteomics. Tissue-based map of the human proteome. *Science* 347: 1260419, 2015. doi:10.1126/science.1260419.

40. **Wan H, Luo F, Wert SE, Zhang L, Xu Y, Ikegami M, Maeda Y, Bell SM, Whitsett JA.** Kruppel-like factor 5 is required for perinatal lung morphogenesis and function. *Development* 135: 2563–2572, 2008. doi:10.1242/dev.021964.

41. **Wang K, Jin X, Chen Y, Song Z, Jiang X, Hu F, Conlon MA, Topping DL.** Polyphenol-rich propolis extracts strengthen intestinal barrier function by activating AMPK and ERK signaling. *Nutrients* 8: 272, 2016. doi:10.3390/nu8050272.

42. **Wiederschain D, Wee S, Chen L, Loo A, Yang G, Huang A, Chen Y, Caponigro G, Yao YM, Lengauer C, Sellers WR, Benson JD.** Single-vector inducible lentiviral RNAi system for oncology target validation. *Cell Cycle* 8: 498–504, 2009. doi:10.4161/cc.8.3.7701.

43. **Wu F, Dassopoulos T, Cope L, Maitra A, Brant SR, Harris ML, Bayless TM, Parmigiani G, Chakravarti S.** Genome-wide gene expression differences in Crohn's disease and ulcerative colitis from endoscopic pinch biopsies: insights into distinctive pathogenesis. *Inflamm Bowel Dis* 13: 807–821, 2007. doi:10.1002/ibd.20110.